UNIVERSITY OF CALIFORNIA
RIVERSIDE

A Study on Spin Current Absorption Through a Transparent Ferro Magnet Junction on Graphene

A Dissertation submitted in partial satisfaction
of the requirements for the degree of

Doctor of Philosophy

in

Electrical Engineering

by

Serol Turkyilmaz

June 2016

Dissertation Committee:
Dr. Mihri Ozkan, Chairperson
Dr. Cengiz Ozkan
Dr. Roger Lake
Dr. Sandeep Kumar

The Dissertation of Serol Turkyilmaz is approved:

_____

_____

_____

_____

Committee Chairperson

University of California, Riverside

Acknowledgements

I would like to thank to my supervisors Dr. Mihri Ozkan and Dr. Cengiz Ozkan for their support throughout my research. I am indebted to my supervisors for letting me pursue a PhD at UCR. I am also grateful to members of my qualifying and PhD defense: Dr. Roger Lake and Dr. Sandeep Kumar and my advisors Dr. Mihri Ozkan and Dr. Cengiz Ozkan.

My sincere gratitude is for our collaborators throughout the C-SPIN project. I would like to specially thank to Dr. Roland Kawakami, Dr. Paul Crowell and Dr. Steven J. Koester for their valuable comments. I am also thankful to my friend Walid Amamou. I really enjoyed the discussions we went through while we were fabricating and measuring spin valves.

I am also very grateful to UCR Nanofab staff members: Mark Heiden, Dr. Dong Yan, and Dexter Humphrey. They were very helpful and did everything to keep the cleanroom operational for our research.

I would like to express gratitude to all of my friends in our research group for their encouragement and support during my PhD work.

I want to thank to my wife Pelin Gokcen Turkyilmaz. She was always supportive, and very understanding. I was always very busy with my PhD studies and working till early mornings in cleanroom all the time since I was also consulting for Oculus-Facebook in parallel to my PhD studies.

Finally, I would like to thank to my parents Serpil and Erol Turkyilmaz for their support throughout my life. They were always supportive and encouraging.

This work was supported in part by C-SPIN, one of the six centers of STARnet, a Semiconductor Research Corporation program, sponsored by MARCO and DARPA.

ABSTRACT OF THE DISSERTATION

A Study on Spin Current Absorption Through a Transparent Ferro Magnet Junction on Graphene

by

Serol Turkyilmaz

Doctor of Philosophy, Graduate Program in Electrical Engineering
University of California, Riverside, June 2016
Dr. Mihri Ozkan, Chairperson

This dissertation consists of 3 different research projects and the first major part is devoted to exploring the spin absorption effect through a transparent Ferro magnet junction on graphene and second major part investigates an advanced nanofabrication technique: multiple angle deposition for the realization of spin transfer torque in graphene lateral non-local spin valve devices in which pure spin current can be produced. A small portion of this thesis is also devoted to the characterization of top gated transistors fabricated on CVD grown and exfoliated MoS_2 film using HfO_2 as a dielectric.

Spin absorption is of current interest for the realization of current induced magnetization reversal of nano-scale magnets which is the key for future spin transfer torque devices. We studied spin absorption by a Permalloy

nanomagnet grown on top of a lateral graphene spin valve channel. A pure spin current is injected into a graphene channel via electrical spin injection through a Co/Al_2O_3 tunnel barrier junction. The Permalloy island in between the injector and the detector is expected to modulate the spin population at the detector via spin absorption. Depending on the magnetization of the Py island, the spin current can be absorbed differently resulting in a distinct signature of non-local magnetoresistance (MR) from the Py island magnetization and hence a modulation of the spin population. We attribute this effect to a combination of both transverse and longitudinal spin current absorptions which is caused by the micro domain formations within the Permalloy island and hence a hysteretic behavior in the MR signal. This hysteretic behavior can be due to the magnetization rotation of micro domains which raise the discussion of both lateral and longitudinal spin absorption. It is very important to investigate the anisotropy of the island and correlate the result to the non-local MR measurement. To this end, magnetic force microscopy of the island is needed in order to further confirm the observed non local signal in our devices. This new effect is still being investigated and further studies are underway to unravel the origin of this new effect observed in graphene spin valves.

Contents

List of Figures

List of Tables

Chapter 1

1.1 Introduction

Transistor based semiconductor devices have been a milestone since the discovery of the transistor in 1947 by William Shockley and coworkers [1]. In the meantime, great success has been achieved in semiconductor industry by CMOS technology and fabrication capabilities [2]. However, semiconductor device technology goes thorough challenges with the drastic increase of power consumption and scaling limits for future devices [3]. Figure 1 shows the trends of physical gate lengths from 2007 to 2021 [4].

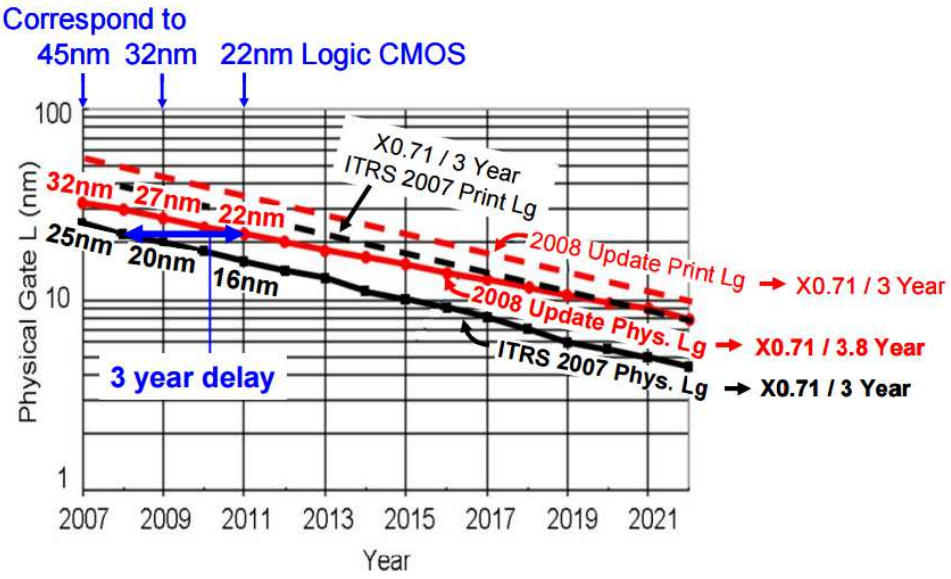

Figure 1.Comparison of ITRS 2007 and 2008, update for the trends of printed (resist) and physical gate lengths. Copyright © [2009] IEEE [4].

The dimensional and equivalent scaling requires additional improvements and adjustments in the individual product and the whole development process with design, material and other structural aspects. These improvements may include investigation of gate stack materials, discovery of new channel materials, and structural modifications (electrostatic control) such as multi-gate field effect transistors [4]. Figure 2 shows the structure and technology innovation for MOSFETs [4].

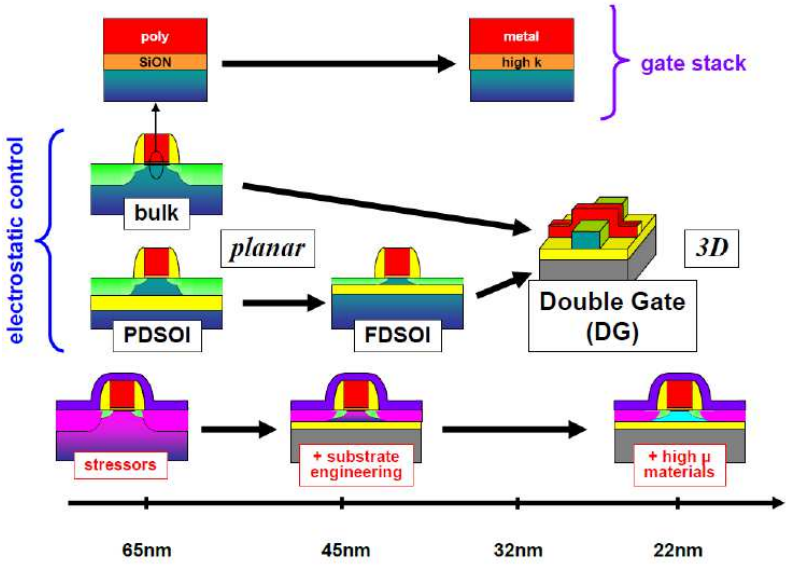

Figure 2. Structure and technology innovation for MOSFETs. Copyright © [2009] IEEE [4].

While recently investigated gate stack materials such as HfO_2 or TiO_2 have higher dielectric constant with respect to SiO_2, many issues need to be resolved in order to employ those as a replacement to SiO_2 [5]. High-K dielectric materials are listed in Table 1 [6].

Table 1. High-K materials and metal gates for CMOS applications. "Reprinted from Materials Science and Engineering R, vol. 88, John Robertson and Robert M. Wallace, High-K materials and metal gates for CMOS applications, pp. 1-41, Copyright (2015), with permission from Elsevier [6].

	K	Gap (eV)	CB offset (eV)
Si		1.1	
SiO_2	3.9	9	3.2
Si_3N_4	7	5.3	2.4
Al_2O_3 sapphire	9	8.8	2.8
Al_2O_3 ALD	8	6.4	1.6
Ta_2O_5	22	4.4	0.35
TiO_2	80	3.5	0
$SrTiO_3$	2000	3.2	0
ZrO_2	25	5.8	1.5
HfO_2	25	5.8	1.4
$HfSiO_4$	11	6.5	1.8
La_2O_3	30	6	2.3
Y_2O_3	15	6	2.3
a-$LaAlO_3$	30	5.6	1.8
$LaLuO_3$	32	5.2	2.1

Likewise, recently discovered 2D channel materials such as graphene, MoS_2, $MoSe_2$ or WSe_2 have issues to be resolved such as process compatibility and process integration despite some of their superior properties when compared to Silicon [7]. On the other side, structural modifications such as multi-gate field effect transistors achieved a great success for suppressing the leakage current by providing gate control from more than one side of the channel when compared to conventional MOSFET [8][9]. Schematic of a classical bulk n-channel MOSFET and a bulk Tri-gate MOSFET are shown in Figure 3 and Figure 4, respectively [9].

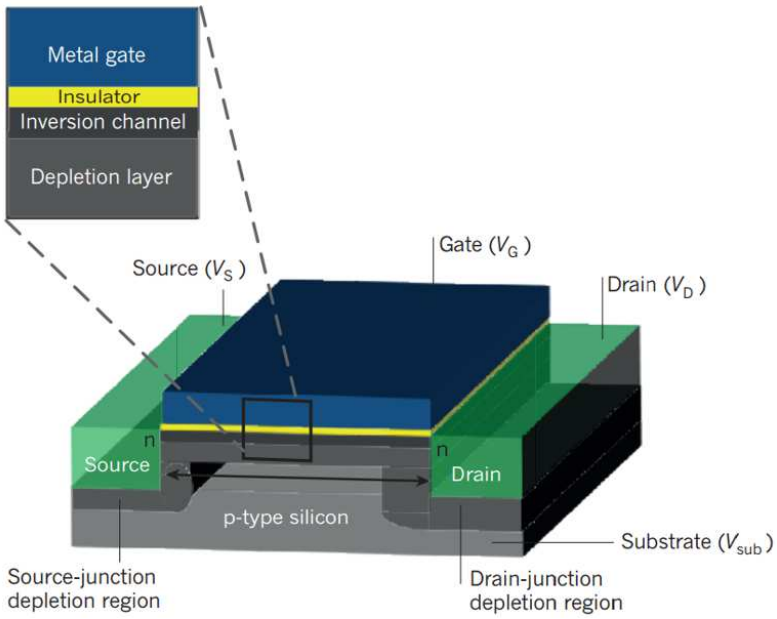

Figure 3. A schematic view of a classical bulk n-channel MOSFET. "Reprinted by permission from Macmillan Publishers Ltd: [Nature] (9), copyright (2011)." [9].

However, discovery of new 2D channel materials, recent developments in gate stack materials and design modifications such as multi-gate field effect transistors may not provide practical value in the long term for addressing the challenges such as scaling limits and drastic increase of power consumption. Drastic increase of power consumption is one of the main reasons that paved the way for the development of non-volatile memory technology. Non-volatile memory can retrieve stored information when the power is turned off while volatile memories like SRAM needs to be powered on for proper operation which results in higher power consumption [10][11]. A six-transistor CMOS SRAM cell is given in Figure 5 [12].

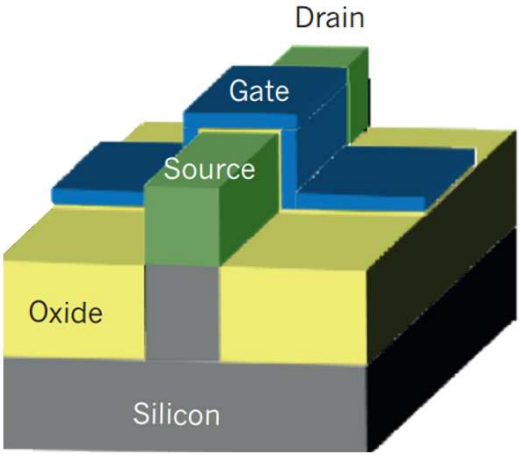

Figure 4. A bulk tri-gate MOSFET. Gate control is exerted on the channel from three sides of the device (the top, the left and the right). “Reprinted by permission from Macmillan Publishers Ltd: [Nature] (9), copyright (2011).” [9].

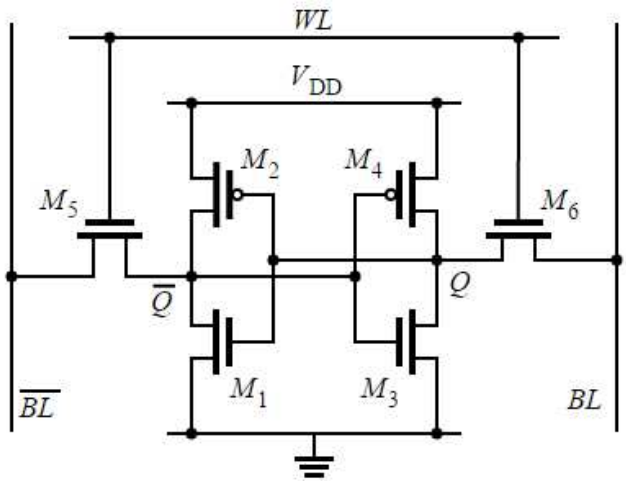

Figure 5. A six-transistor CMOS SRAM cell. Reprinted from Wikipedia [12].

Recent progresses in non-volatile memory research focus on Phase-change RAM, Ferroelectric RAM, and Magnetic RAM [13]. Phase-change RAM relies on phase change materials that can store and release large amount of energy by heat exchange. Heat exchange causes phase change between amorphous and crystalline which results high and low resistivity,

respectively [14][15]. Change in the resistance is used to store binary states in the cell. However, since the access latency is the limiting factor, further development is needed for phase-change RAM technology. Ferroelectric RAM uses a ferroelectric layer acting as a ferroelectric capacitor of which spontaneous electric polarization can be reoriented by applying a static electric field. Non-volatility is achieved due to the spontaneous electric polarization within the ferroelectric material [16]. Magnetic MRAM is of current interest due to desirable features such as high endurance, high speed reading/writing and low power consumption [17]. MRAM uses magnetic moments of electrons to store data instead of electrical charges when compared to DRAM or SRAM [18].

The origin of information storage with magnetic charges dates back to 1980s when giant magnetoresistance was first discovered by Grunberg and Fert [19][20]. The discovery paved the way for development of GMR recording heads for hard disk drives whose working principle is based on spin dependent scattering of electrons in a special structure called spin valve [21][22][23]. A spin valve is a device in which high and low electrical resistance states can be realized using the relative alignment of the magnetization in the magnetic layers [24]. Great success has been achieved in hard disk drives using spin valve/GMR recording heads in the meantime and potential applications are quickly recognized in other fields such as magnetic field sensing and non-volatile memory applications

[25][26][27]. Based on the spin dependent scattering of electrons, non-volatile memory can be realized in two ways very briefly; magnetic tunnel junctions and lateral spin valves [28][29][30]. In magnetic tunnel junctions, spin current flows together with charge current which causes joule heating [31]. On the other side, in lateral spin valves spin current is isolated from charge current and is of current interest due to low power consumption and elimination of joule heating. However, realization of current induced magnetization switching is harder in lateral spin valve due to pure spin current switching and further improvement is needed in order to employ spin transfer torque (STT) in non-local spin valve geometry for the realization of current induced magnetization reversal [32][33]. Schematic of non-local spin transport measurement for a lateral spin valve is shown in Figure 6.

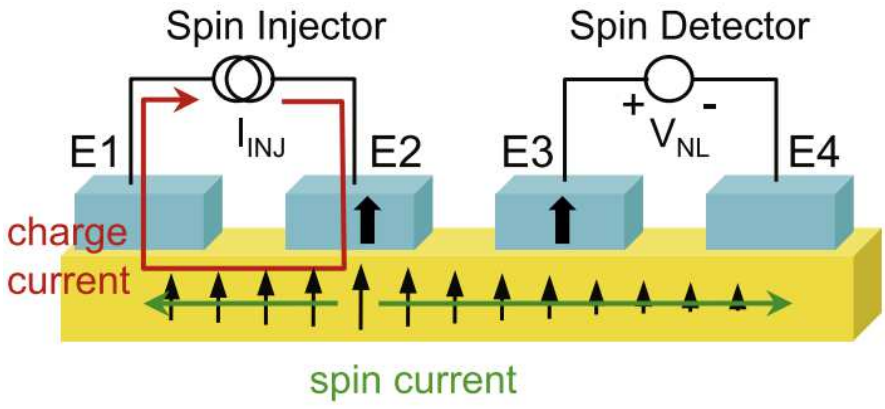

Figure 6. Schematic of non-local spin transport measurement. “Reprinted from Journal of Magnetism and Magnetic materials, vol. 324, no. 4, Wei Han, K.M. McCreary, K. Pi , W.H. Wang, Yan Li, H. Wen, J.R. Chen, R.K. Kawakami, Spin transport and relaxation in graphene, pp. 369-381, Copyright (2012), with permission from Elsevier.” [34].

In conclusion, Spintronics may provide practical value for post-complementary metal-oxide-semiconductor (CMOS) technology and can be employed as a replacement to current CMOS devices in the long term. This can be achieved by either with MTJ or lateral spin valve geometry using spin current to carry information and realize the current induced magnetization reversal via spin transfer torque [32]. STT-RAM (Spin Transfer Torque RAM) should have better scalability to be considered as a promising candidate for future devices. Besides, good CMOS compatibility and process integration issues should also be resolved in order to employ STT-RAM as a replacement to charge based CMOS technology and devices [35].

1.2 2D materials

Regardless of the discoveries in science and changes in technology, materials have always played a critical role in shaping the development of our civilization such as semiconductor materials which have been the foundation of modern electronics. The search for new semiconductor materials became an active research area today [36][37][38]. Recently, 2D materials attracted massive attention due to their superior properties and promising applications for future semiconductor device applications [39]. This section discusses the (2DLMs) two-dimensional layered materials and provide substantial knowledge about superior properties and

characteristics of currently investigated two-dimensional layered materials and TMDs (The transition metal dichalcogenides).

Two-dimensional layered materials can be defined as single/multi-layer materials which can be obtained by cleavage due to strong in-plane chemical bonds and weak coupling between the layers [40][41]. 2D materials attracted much interest by the discovery of graphene and ignited intensive interest due to exceptional electrical, chemical and physical properties [42]. Synthesis and growth of 2D materials also attracted much attention due to recent advances and motivation for growing complex hetero-structures and large-scale films for device applications [43][44]. TMDs on the other hand are atomically thin semiconductors and may exhibit tunable band gap which can crossover from indirect to direct when scaled down to single layer for certain materials [42][45][46].

Among two-dimensional layered materials, graphene was discovered by Andre Geim and coworkers in 2004 [47]. Graphene is the single layer form of graphite and can be obtained by exfoliation technique using adhesive tape [48]. Single layer graphene can be achieved by repetitive peeling steps and Si wafer with a 300 nm SiO_2 layer provide the optical detection of graphene flakes which is required for further device fabrication steps [49][50]. The importance of single layer graphene comes from its unique electrical properties [51]. It is discovered that when graphite goes down to single atomic layer, its electrical properties show promising characteristics

for future nano electronic devices [52][53]. Graphene has Dirac delta function different than other 2D materials which makes it special [47]. It has a high electron mobility of 200,000 cm^2/Vs in theoretical [53]. A mobility value of 200,000 cm^2/Vs has been achieved by suspended single layer graphene which is achieved by 1:6 buffered oxide etch (BOE) of SiO_2 layer [54]. Another study has reported a mobility value of 8500 cm^2/Vs by contactless top gate FETs [55]. Contactless top gates are realized on graphene layers using LOR resist which eliminates the pinholes and dielectric breakdown. LOR and PMMA resists are developed with MIBK and MIF319 developers. Metals are evaporated with 45^o and -45^o for the full coverage of the sidewalls and edges. Suspended structure is released after the lift-off process. Basic circuitry operation has also been achieved using p and n type graphene transistors [56][57]. Schematic of an integrated complementary graphene inverter with scanning electron microscopy image and the circuit layout are given in Figure 7. Complementary behavior is realized in the range between Dirac points [56]. Inverter is fabricated by employing two FETs based on monolayer graphene. While both of the FETs show p type behavior at small gate voltages, type inversion is occurred after $V_G = 13.9$ V. While R_n refers to the left transistor, R_p corresponds to the right transistor and transistors exhibits complementary behavior between Dirac points [56]. Despite its high electron mobility and functionality for analog device applications, the lack

of the band gap in graphene leads to low on/off current ratio typically 100 in top gated graphene FETs at room temperature [57].

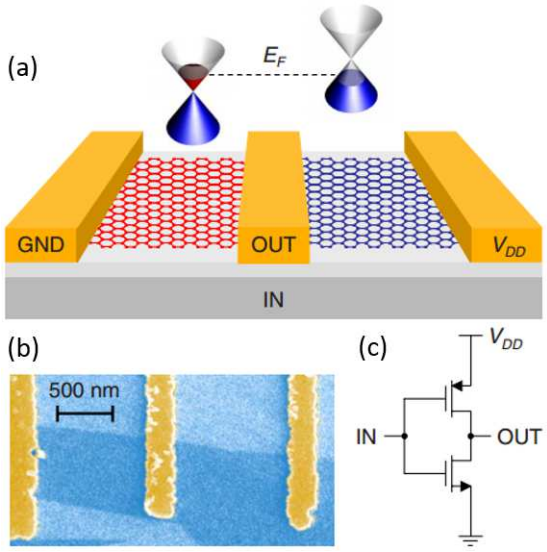

Figure 7. Integrated complementary graphene inverter (a) A schematic of the fabricated inverter. (b) Scanning electron microscopy image of the fabricated inverter (c) The circuit layout. “Reprinted from [F. Traversi, V. Russo, and R. Sordan, “Integrated complementary graphene inverter,” Appl. Phys. Lett., vol. 94, no. 22, pp. 223312, 2009.] with the permission of AIP Publishing.” [56].

Thus, graphene is not a promising candidate as an effective field effect transistor for digital electronic applications due to low on/off current ratios caused by the lack of band gap [57][58]. Introducing band gap to graphene is achieved in 2010 by processing graphene sheets into nanoribbons using block copolymer lithography [59]. This technique can introduce band gap even into large scale graphene sheets and high current on/off ratios can be achieved with a significant decrease in electron mobility. All in all, graphene is not a good candidate for effective field effect transistor in digital electronic applications due to lack of band gap and low

current on/off ratio. This resulted in an increasing interest in TMDs such as MoS_2 or WSe_2. MoS_2 (Molybdenum disulfide) is an inorganic compound and crystals of MoS_2 are composed of molybdenum and sulfur atoms. Weak interaction forces allow separation of layers by exfoliation or mechanical cleavage [60][61] and mono layer MoS_2 has a direct band gap while the bulk form is an indirect semiconductor [62]. In contrary to graphene, MoS_2 showed promising electrical characteristics for use as efficient field effect transistor in digital electronics and provide practical value in sensing applications [63][64]. The first field effect transistor is reported by B. Radisavljevic in 2011 based on single layer MoS_2 flake, demonstrated a mobility of 200 cm^2/Vs and a current on/off ratio of $1x10^8$ using Hafnium oxide (HfO_2) as gate insulator [65]. Cross sectional view of the monolayer MoS_2 FET and transfer characteristic are given in Figure 8.

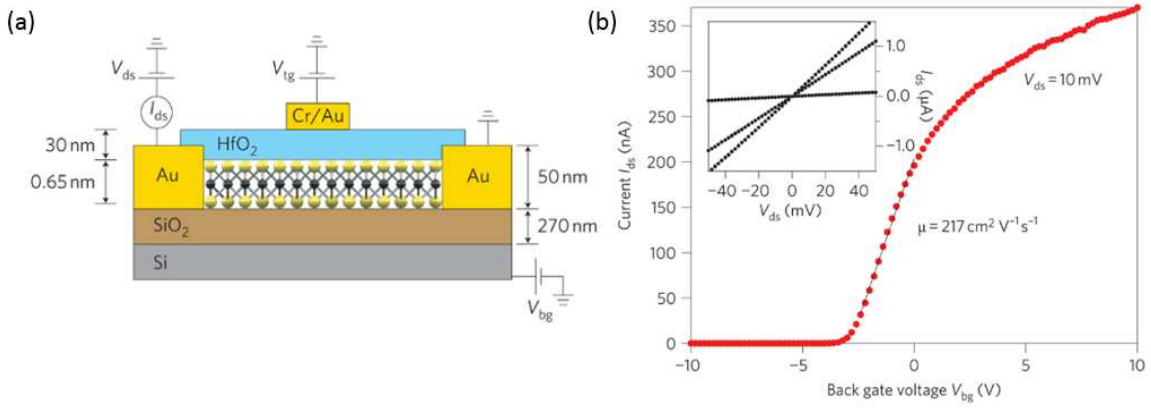

Figure 8. (a) Cross sectional view of the structure of a monolayer MoS_2 FET. (b) Room-temperature transfer characteristic for the FET with 10 mV applied bias voltage V_{ds}. "Reprinted by permission from Macmillan Publishers Ltd: [Nature Nanotechnology] (65), copyright (2012)." [65].

High on/off ratios make MoS_2 such an attractive material for the realization of logic operations [66]. Cross-sectional view of the monolayer MoS_2 integrated circuit and output voltage as a function of the input voltage are given in Figure 9. Despite its high on/off ratios, replacement with Silicon is still in question due to process compatibility and process integration issues.

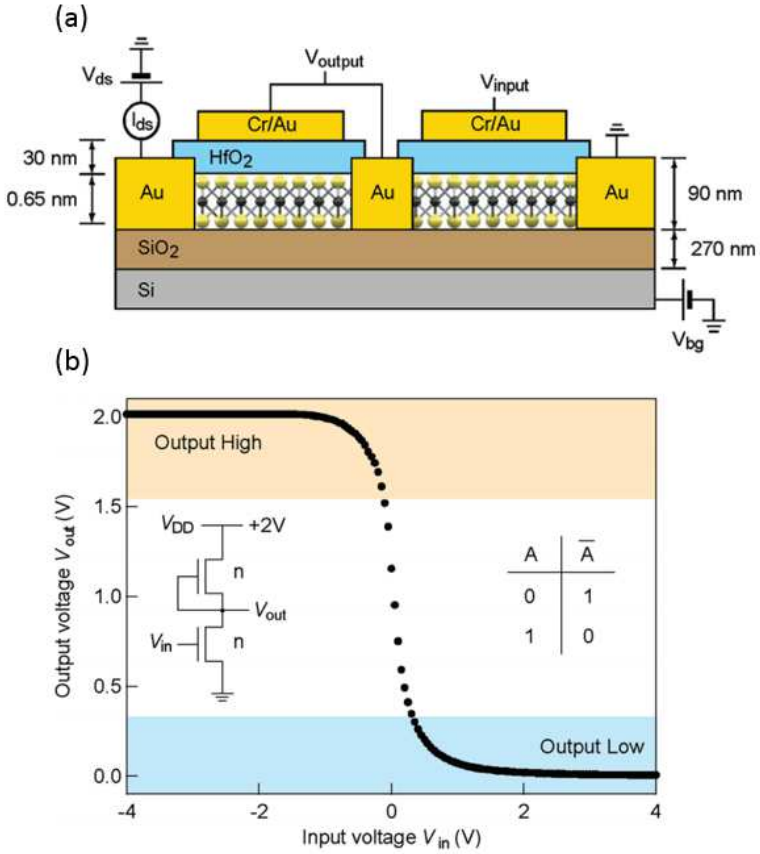

Figure 9. (a) Cross-sectional view of the structure of a monolayer MoS_2 integrated circuit (b) Output voltage as a function of the input voltage. "Reprinted (adapted) with permission from (B. Radisavljevic, M. B. Whitwick, and A. Kis, "Integrated circuits and logic operations based on single-layer MoS_2.," ACS Nano, vol. 5, no. 12, pp. 9934–8, Dec. 2011.). Copyright (2011) American Chemical Society." [66].

WSe_2 is another layered semiconductor with a hole mobility of 250 cm^2/Vs measured with a top gated design based on a single layer WSe_2 film using chemically doped contacts and with high k dielectric [67]. Schematic of the top-gated WSe_2 monolayer FET and transfer characteristic are shown in Figure 10. The fabricated top gate transistor exhibit a current on/off ratio of 10^6 and reduction in contact resistance is achieved by NO_2 chemical doping resulted in a p type behavior with excellent characteristics.

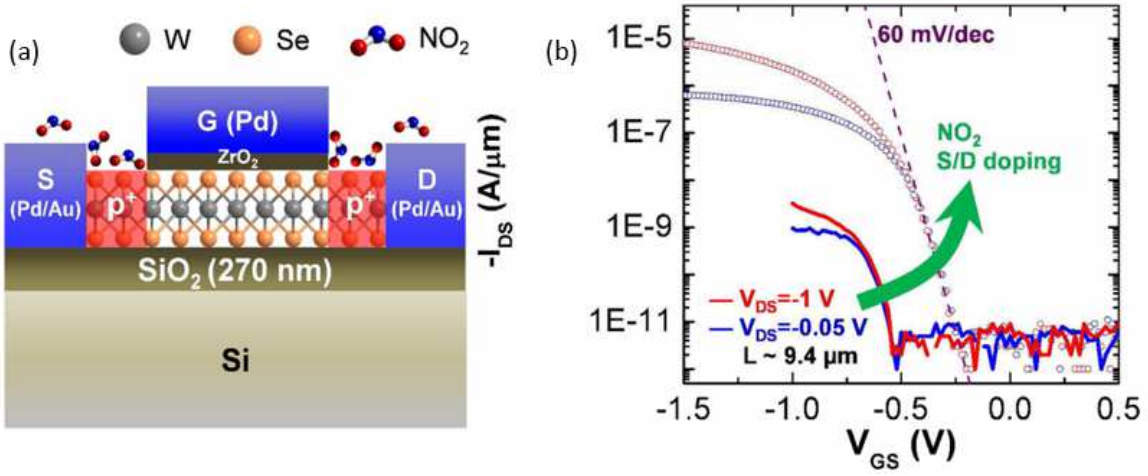

Figure 10. (a) Schematic of a top-gated WSe_2 ML-FET with chemically p-doped S/D contacts by NO_2 exposure (b) Transfer characteristics of a device with L of ~9.4 μm before and after NO_2 patterned doping of the S/D contacts. "Reprinted (adapted) with permission from (H. Fang, S. Chuang, T. C. Chang, K. Takei, T. Takahashi, and A. Javey, "High-performance single layered WSe_2 p-FETs with chemically doped contacts.," Nano Lett., vol. 12, no. 7, pp. 3788–92, Jul. 2012). Copyright (2012) American Chemical Society." [67].

In conclusion, process compatibility and integration issues remain to be resolved for the integration of 2D materials into CMOS processes. However,

Spintronics is another promising candidate to solve the scaling issues and power consumption problems beyond 2025 and non-volatile spin logic may overtake charge based binary logic approach [68][69][70]. The history of spintronic goes back to the discovery of the giant magneto resistance effect found by Fert and Grunberg independently in 1988 [71][72]. Spin based research attracted much attention since then and spin valves have been extensively studied to understand the spin properties of semiconductors and new channel materials. Starting from the brief history of magnetism, next section will discuss Spintronics with a focus on lateral spin valves and spin transfer torque in graphene.

1.3 Spintronics

Spintronics is the study of the intrinsic spin of the electron instead of or in addition to the charge of electrons and has attracted much attention during the last decades because of its potential applications both in information storage and post complementary CMOS devices [73][74][75]. However, history of Spintronics dates back to 1st centuries BCE since Spintronics basically originates from magnetism. Magnetism was first described as mysterious attraction thousands of years ago and discovered with Magnetite which is a type of rock with the chemical formula "Fe_3O_4" [76][77]. Magnetism was first mentioned in De Rerum Natura (On the Nature of things) by poet Lucretius in the 1st century BCE as a propelling force by which iron atoms flow out and sucks other materials creating a

vacuum [77]. It would take centuries to understand this mysterious force and the first application would come out as the magnetic compass. Today, we have gained much understanding of magnetism through the developments in science and great progress has been achieved especially after the discovery of the relationship between electricity and magnetism. Today, we know much more about magnetism and are aware of why certain materials can be magnetized while others cannot. We also understand the origin of the magnetism which is basically spin of electrons that tend to align with each other [78]. An electron has two different intrinsic properties. One of them is the electronic charge property while the second one is the intrinsic spin of the electrons [79]. Electron spin is the fourth quantum number for electrons in atoms and denoted by either upward or downward as schematically shown in Figure 11 [80].

Spintronics is based on the spin dependent density of states of the ferromagnetic materials [81]. Ferromagnetic materials play a significant role in spin transport and magnetism due to the energy difference between spin up and spin down states [82]. This results in different scattering environment for electrons at different spin states which results in a spin polarized current when an electrical current flows through a ferromagnetic material. The electronic density of states within a ferromagnetic material becomes spin dependent under a magnetic field which allows spin injection and detection throughout ferromagnetic materials [83]. Spin

dependent density of states for a ferromagnetic and nonmagnetic metal is shown in Figure 12.

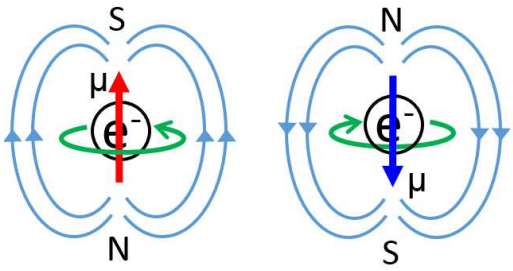

Figure 11. The magnetic spin of an electron in the direction of magnetic field lines. “Adapted from General Chemistry, 3rd edition, by Hill and Petrucci and "Electricity and Magnetism: Berkeley Physics Course," vol. 2, 2nd ed., by Edward M. Purcell.” [80].

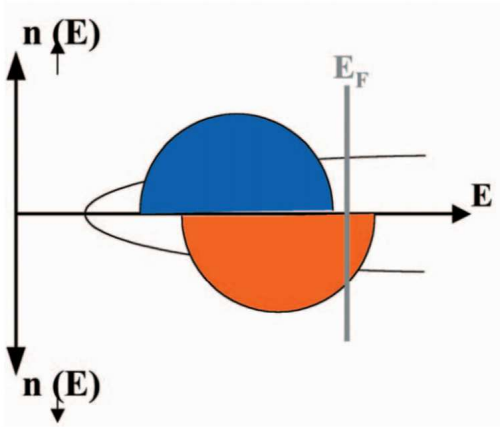

Figure 12. Typical band structure of a ferromagnetic metal. Modified from [84]. “Reprinted (Figure 1-a) with permission from [Albert Fert, Reviews of Modern Physics, Nobel Lecture: Origin, development, and future of spintronics, vol. 80, pp. 1517-1530, 2008] Copyright (2008) by the American Physical Society.” [84].

Spin based research attracted much attention after the discovery of the giant magneto resistance effect [71][72] and spin valves have been extensively studied to understand the spin properties of semiconductors and new channel materials [85][86]. Figure 13 shows the giant

magnetoresistance effect discovered in FM/NM multilayers. Ferromagnetic layers align in anti-parallel configuration when the non-magnetic layer is selected to be very thin due to RKKY coupling in between the adjacent FM layers [87]. GMR amplitude as a function of the non-magnetic layer thickness is given in Figure 14.

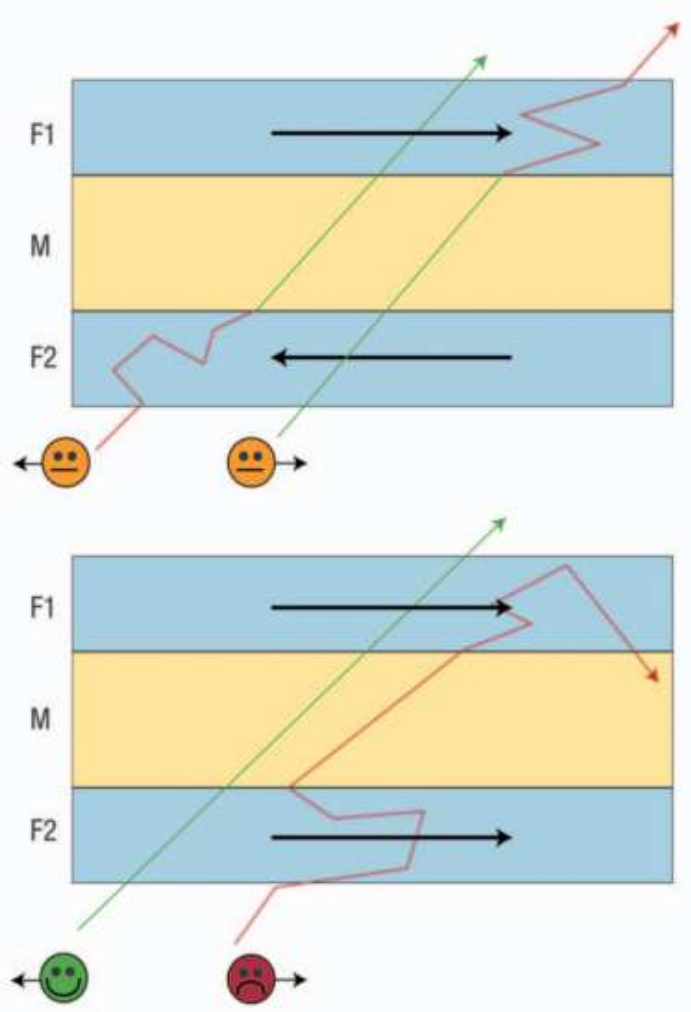

Figure 13. Giant magnetoresistance effect in thin film structures. "Reprinted (Figure 3-c) with permission from [Albert Fert, Reviews of Modern Physics, Nobel Lecture: Origin, development, and future of spintronics, vol. 80, pp. 1517-1530, 2008] Copyright (2008) by the American Physical Society." [84].

A magnetic field is able to change the magnetization of adjacent FM layers from anti-parallel to parallel configuration. Anti-parallel configuration results in high electrical resistance while parallel configuration results in low electrical resistance [88][89]. This useful property in thin film structures opened a wide variety of applications for GMR sensors including magnetic field sensors and write/read heads for hard disk drives [90]. Schematic drawing of a spin valve read element and shielded sensor are given in Figure 15.

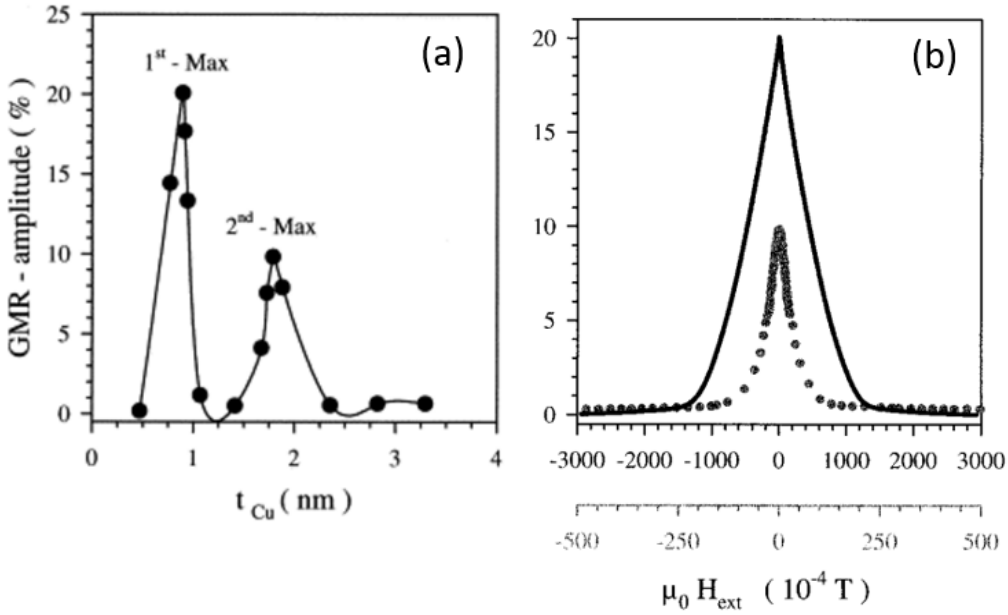

Figure 14. (a) Room-temperature amplitude of magnetoresistance as a function of the Cu spacer layer thickness for a series of multilayers of the form $Py_{1.9nm}//\{Cu_{tnm}/Py_{1.6nm}\}_{40}$. (b) Room-temperature magnetoresistance vs field curves at the 1st (solid black line) and second (dotted gray line) antiferromagnetic coupling maximum. "Reprinted from Acta Materialia, vol. 47/no. 15-16, A. Huétten, S. Mrozek, S. Heitmann, T. Hempel, H. Bruéckl and G. Reiss, Evolution of the GMR-effect amplitude in Copper/Permalloy-Multilayered thin films, pp. 4245-4252, Copyright (1999), with permission from Elsevier." [89].

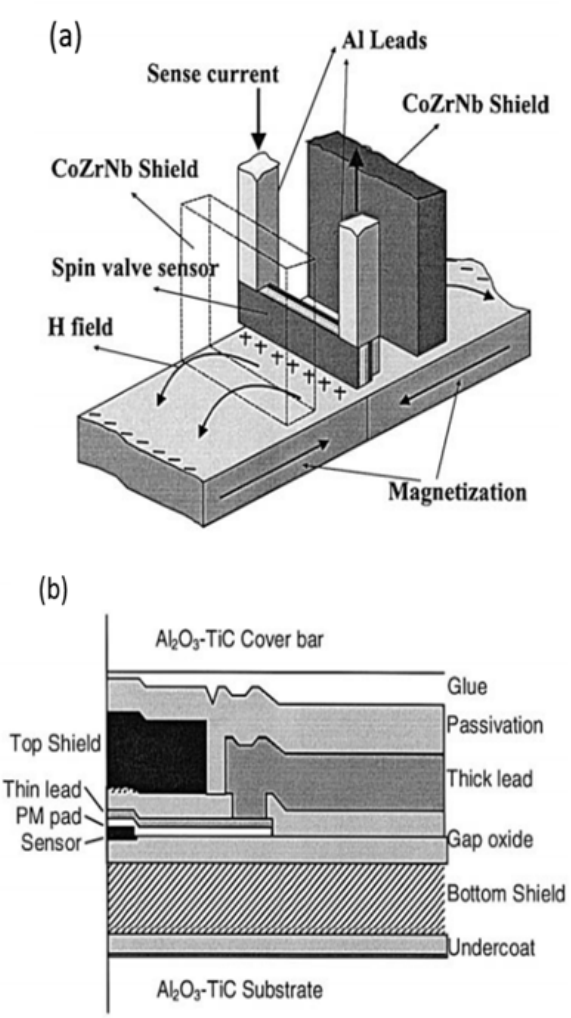

Figure 15. (a) Schematic drawing of a spin valve read element in a tape recording head. (b) Schematic drawing of a shielded sensor stabilized with overlaid CoCrPt permanent magnets. "Reprinted from Sensors and Actuators A: Physical, vol. 81 /no. 1-3, P.P Freitas, F Silva, N.J Oliveira, L.V Melo, L Costa, N Almeida, Spin valve sensors, pp. 2-8, Copyright (2000), with permission from Elsevier." [92].

In conclusion, Spintronics is an emerging field and find applications with the current developments both in information storage and semiconductor industry. For the last 3 decades, spin valves and GMR sensors are extensively studied to understand the spin dependent properties of new

materials which also raised an interest in emerging applications such as magnetic tunnel junctions. However, this study focus on graphene spin valves and the emphasis will be given to the lateral spin valves and spin absorption in graphene.

1.4 Spin Valves

A spin valve can be described as a magnetic field sensor which uses the intrinsic property of electron called spin [93][94]. Since electron spin is quantized, it can have either up or down state depending on the applied magnetic field or exchange interactions which constitutes the fundamental operation principle of spin valves [94][95]. Considering the design geometry, spin valves can be classified into two groups; current perpendicular to plane (CPP) geometry in which current is passed perpendicular to the layers and current in plane (CIP) geometry in which current flows along the layers [74]. CPP and CIP geometry can also be referred as vertical and lateral spin valve, respectively. CPP and CIP geometries are both shown in Figure 16. In vertical spin valve design, spin transport channel is sandwiched in between two ferromagnetic electrodes. Spin transport and detection is achieved by injecting spin polarized electrons from one electrode and detecting spins from the second electrode. In lateral spin valve, ferromagnetic electrodes are defined on spin transport channel [96][97].

There are two geometries for measuring magnetoresistance in lateral spin valves [98][99]. The first one is the local magnetoresistance geometry in which the resistance is measured across the two ferromagnetic electrodes. The second one is the non-local magnetoresistance geometry in which spin polarized electrons are injected from one electrode, and detected by another pair of electrodes. Spin transport is detected as the difference in resistance depending on the parallel or anti-parallel magnetization alignment of electrodes [100]. Local measurement uses two ferromagnetic electrodes while non-local measurement uses four electrodes of which inner ones need to be ferromagnetic for spin injection and detection. In local MR measurement, spin current is not isolated from the charge current and is less sensitive to detect the spin signal. On the other side, non-local measurement technique is more sensitive with higher signal-to-noise ratio when compared to local-measurement technique [101]. Non-local measurement geometry can be easily realized using lateral spin valve geometry while it is more difficult to realize using CPP geometry in practice when compared to CIP configuration. However, vertical spin valves find applications in building high density non-volatile memory using local measurement technique [102][103].

For non-local measurement, spin injection is achieved by connecting a current source across the left two electrodes, while spin detection is achieved across the right two electrodes. Injected spins diffuse in both

directions and spin density decays due to spin-flip scattering. In a lateral graphene spin valve, spin flip scattering mechanism is explained by Elliot-Yafet or Dyakonov-Perel spin relaxation mechanisms [104][105][106]. Voltage will be positive for the parallel alignment and negative for anti-parallel alignment of the electrodes. Thus, the signal generated by the spin transport is the non-local MR defined by

$$\Delta R_{NL} = \frac{V_P - V_{AP}}{I}$$

where I is the injection current. V_p is the potential difference when magnetization of electrodes is in parallel configuration and V_{ap} is the potential difference when magnetization of the electrodes is in anti-parallel configuration [104]. Optical image of a graphene spin valve and non-local MR loop is given in Figure 17.

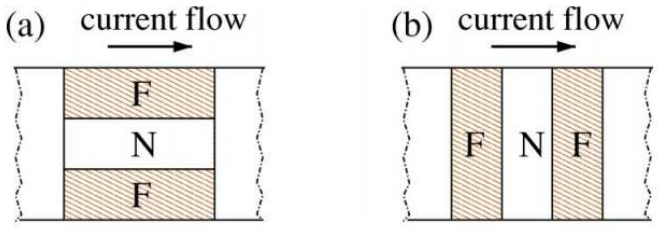

Figure 16. Schematic illustration of (a) the current in plane (CIP), (b) the current perpendicular to the plane (CPP) giant magnetoresistance geometry. "Reprinted (Figure 3) with permission from (Igor Žutić, Jaroslav Fabian, and S. Das Sarma, Reviews of Modern Physics, Spintronics: Fundamentals and applications, vol. 76, pp. 327, 2004.] Copyright (2004) by the American Physical Society)." [74].

Figure 18 shows the detailed schematic of a lateral spin valve with non-local MR measurement geometry while Figure 19, 20 and 21 describes the

relationship between the configurations of ferromagnetic electrodes with the MR signal.

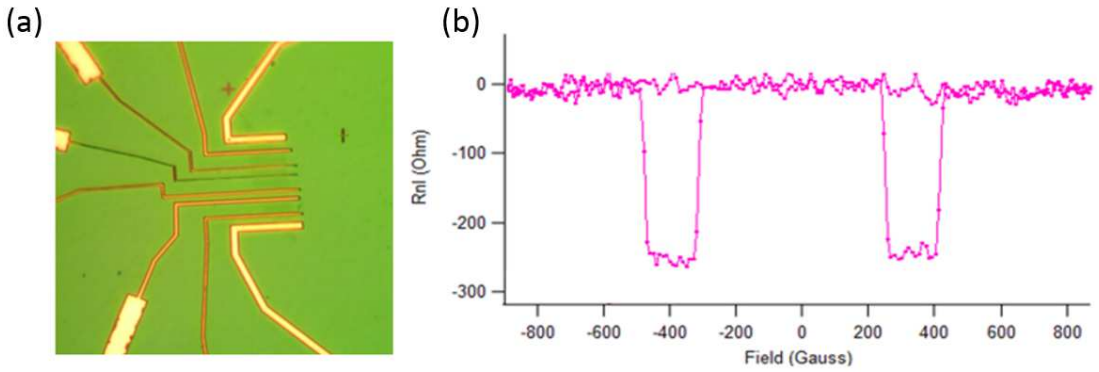

Figure 17. (a) Optical image of the graphene lateral spin valve (b) Nonlocal MR loop for the graphene lateral spin valve.

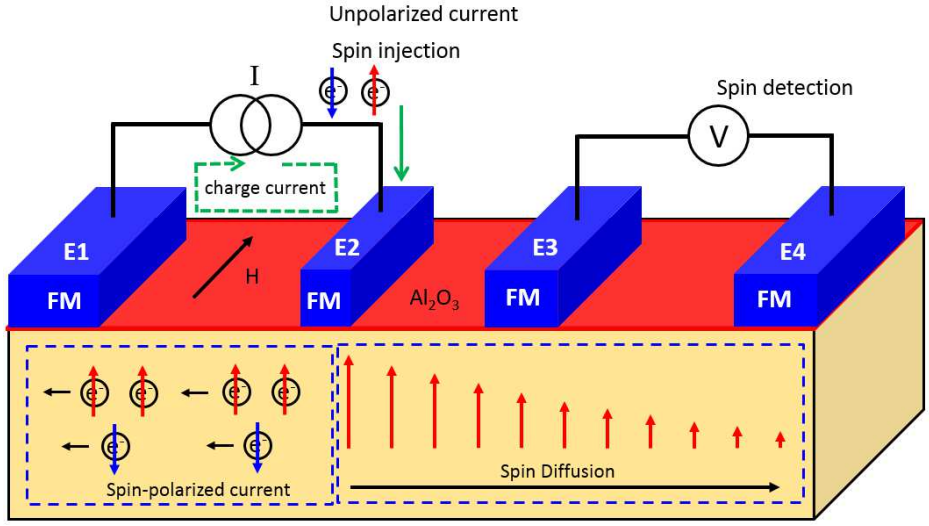

Figure 18. (a) Lateral spin valve with non-local magnetoresistance measurement geometry.

Un-polarized electrical current is injected through E2 and non-local magnetoresistance is measured through E3 and E4 while an in-plane magnetic field is applied simultaneously. Co electrodes switch magnetization direction depending on the magnetic field intensity. Width

of each electrode is defined differently to obtain distinct coercive fields. This is crucial for the MR measurement. Polarized electrical current is produced in the transport channel through spin injection due to spin dependent density of states of the ferromagnetic Co electrode.

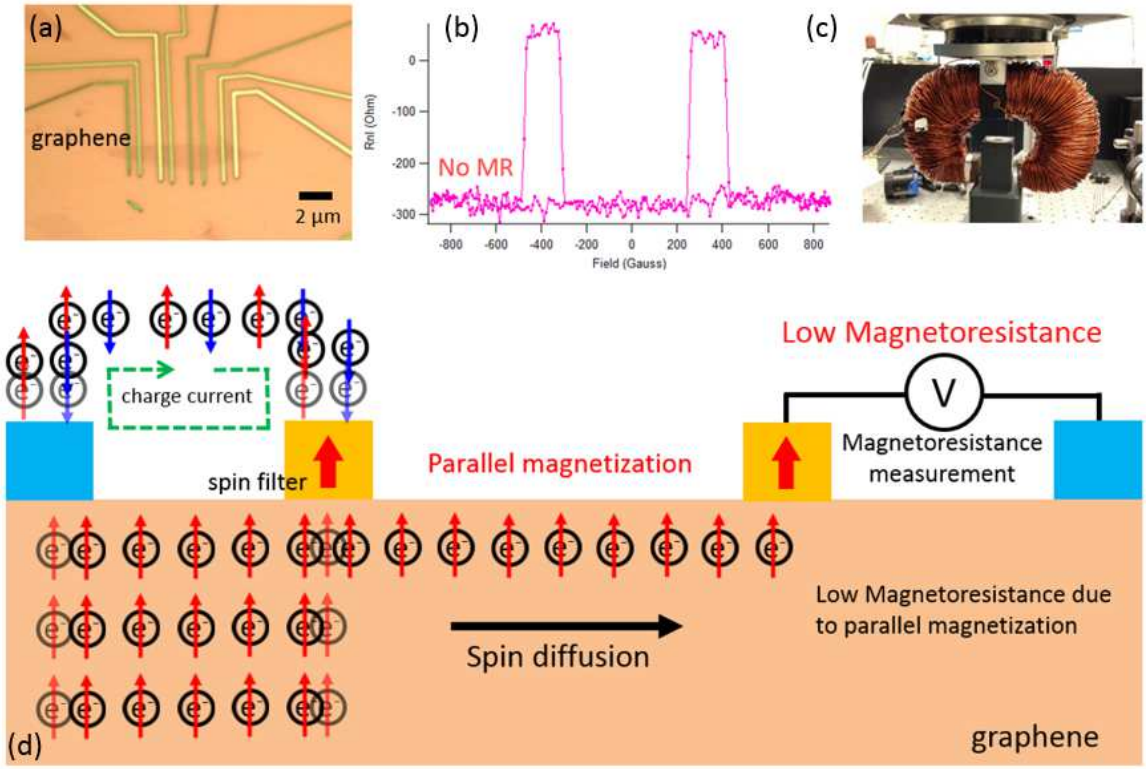

Figure 19. (a) Optical image of a lateral spin valve (b) Non-local magnetoresistance measurement (c) Electrical current driven home made magnet (d) Lateral spin valve operation principle.

Measurement starts with the application of an in-plane magnetic field and magnetic field is swept from negative to positive field. Magnetization of each cobalt electrode is switched at different magnetic fields due to distinct coercive fields. Simultaneously, charge current is injected from electrode E2.

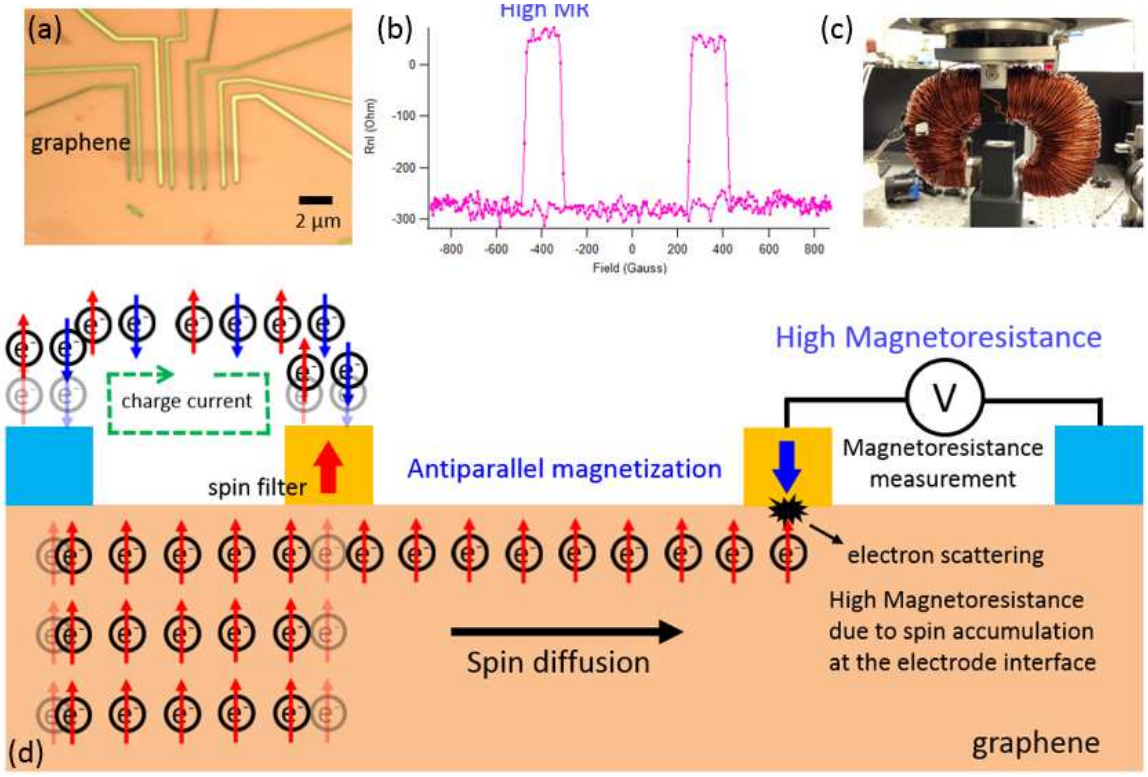

Figure 20. (a) Optical image of a lateral spin valve (b) Non-local magnetoresistance measurement (c) Electrical current driven home made magnet (d) Lateral spin valve operation principle.

Basically, we have a current loop of spin polarized current in the graphene channel in between two electrodes. Concurrently, spin dependent chemical potential is measured from the right electrodes. When the inner electrodes are in parallel configuration, there is no MR. High MR is measured when they are in anti-parallel configuration due to spin accumulation underneath the E3 electrode. Non-local MR is measured because of the change in spin dependent chemical potential due to spin scattering at the electrode interface.

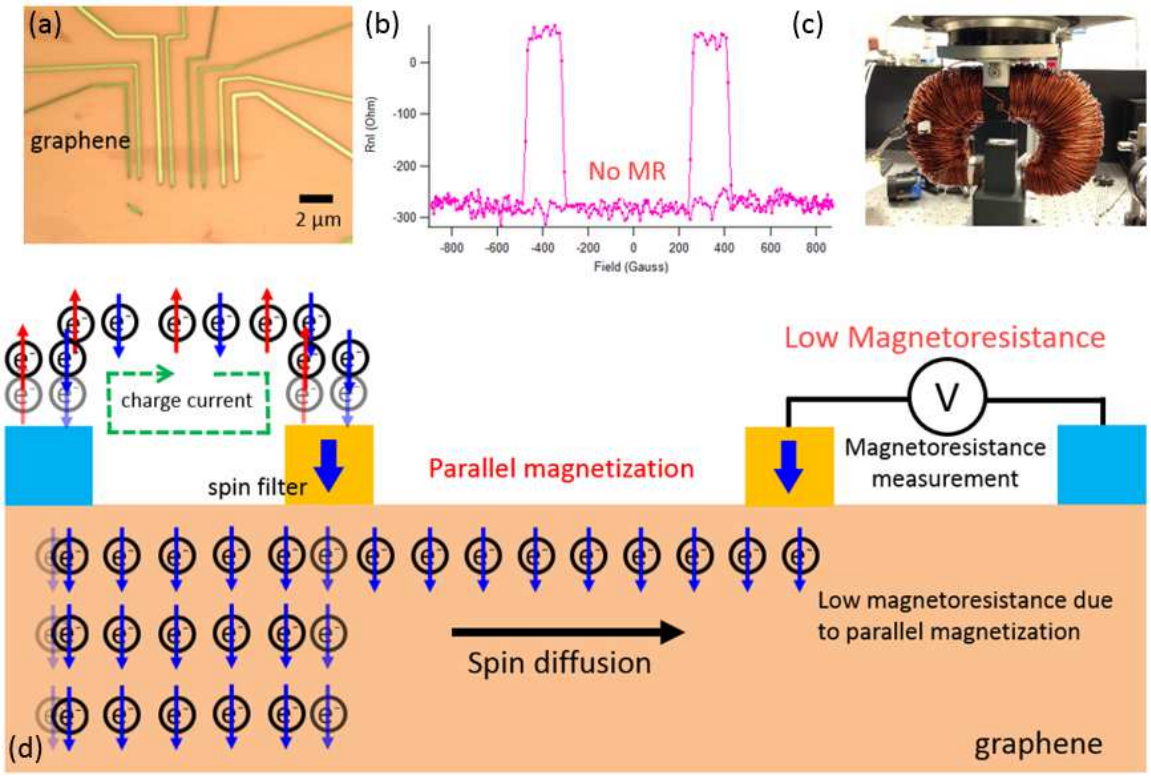

Figure 21. (a) Optical image of a lateral spin valve (b) Non-local magnetoresistance measurement (c) Electrical current driven home made magnet (d) Lateral spin valve operation principle.

1.5 Review of spin valves

The first spin injection and detection is achieved in 1985 through a single crystal aluminum bar after 9 years when first electronic spin injection idea was proposed by the first time in 1976 [107][108]. Spin injection and transport has been widely studied in nonmagnetic metals in the meantime [85][86]. However, compared to the metal based spin valves, it is discovered that semiconductors have longer spin lifetimes [109]. Thus, semiconductors have attracted great interest as a spin transport channel material. However, the expected impact cannot be achieved at the first

glance due to the conductivity mismatch problem between FM material and the semiconductors [110]. This problem was solved by using a Schottky barrier or an oxide tunneling barrier [111]. The first spin injection and detection in semiconductors was achieved in 2007 using a Fe/GaAs Schottky barrier [112]. In 2009, silicon is used as a spin transport channel and spin injection is achieved at room temperature [113]. All in all, spin injection and transport have been demonstrated both in metals and semiconductor materials [113][114]. However, carbon based materials have attracted significant attention due to high spin diffusion length, long spin lifetimes and low intrinsic spin orbit coupling [115]. Graphene has drawn more attention due to its high mobility and easy controllability of carrier concentration [116][118]. Several groups have shown spin injection and transport in graphene using lateral spin valve geometry [99][117][118][119]. Scanning electron micrograph of a four-terminal single-layer graphene spin valve and non-local measurement are given in Figure 22.

In a lateral spin valve, ferromagnetic electrodes are defined on spin transport channel and spin polarized electrons are injected from one electrode and diffuse towards the detector electrode by which the spin accumulation is measured [104]. Lateral spin valves are in current interest for spin transfer torque and spin absorption due to the isolation of spin current from the charge current in order to eliminate the joule heating

which is a drawback in magnetic tunnel junctions [120]. This is due to the CPP geometry of magnetic tunnel junctions in which spin current flows together with the charge current. This causes joule heating which is a drawback for the realization of STT-MRAM [31]. Instead, joule heating can be eliminated using only pure spin current in a lateral spin valve geometry for the realization of spin transfer torque effect.

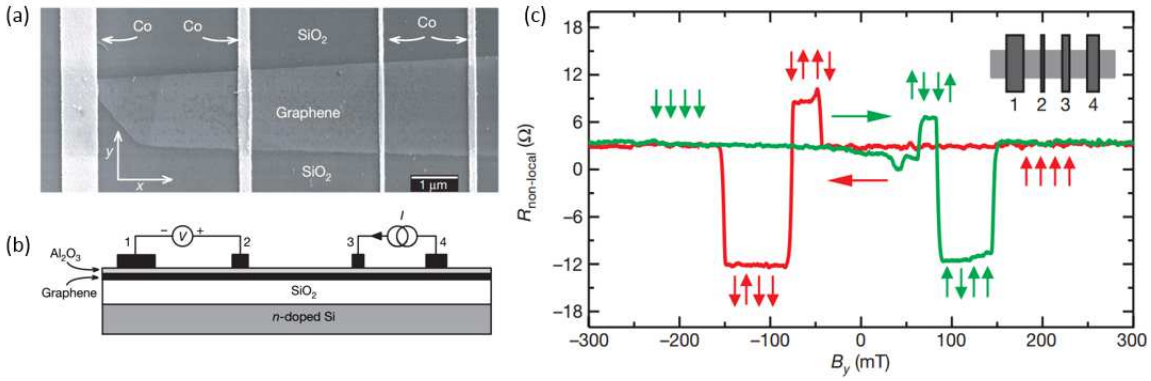

Figure 22. (a) Scanning electron micrograph of a four-terminal single-layer graphene spin valve (b) The non-local spin valve geometry (c) Non-local spin valve signal at 4.2K. “Reprinted by permission from Macmillan Publishers Ltd: [Nature] (Tombros, Nikolaos, et al. "Electronic spin transport and spin precession in single graphene layers at room temperature." Nature 448.7153 (2007): 571-574.), copyright (2007).” [99].

1.6 Spin absorption

Pure spin current can be captured using non-local geometry in lateral spin valves and spin absorption is of current interest for the realization of current induced magnetization reversal of nano-scale magnets which is the key for future spin transfer torque devices. Collinear configuration of injector and detector electrodes were used for investigating the transverse and longitudinal spin current absorption [120]. Longitudinal and

transverse spin absorption into a Permalloy nanowire was studied in a lateral spin injection device with a V-shaped ferromagnetic injector and detector. It has been found out that the spin absorption efficiency depends on the relative angle orientation of the injected spin current and the magnetization of the spin absorber [120]. Scanning electron microscope image of the Py/Cu lateral spin valve and transverse and longitudinal configuration are given in Figure 23 [120]. Corresponding non-local MR signal and schematic illustrations for the domain structures of the V-shaped injector, detector, and absorber are shown in Figure 24. Quantitative examination states that spin absorption for transverse spin current is higher based on the angular dependence measurement [120]. This is due to the different spin polarization in transverse and longitudinal configuration which results in different spin resistance and so the spin absorption efficiency [121]. Schematic view of the non-local spin valve with three ferromagnetic layer showing the dependence of the magnetoresistance on the relative angle between injector and absorber is given in Figure 25 [121].

Extensive studies in spin absorption effect plays an important role in discovering the spin physics for pure spin current induced magnetization switching for future spin transfer torque devices. There has been great interest in spin transfer torque due to its potential device applications

since it was first proposed in 1996 for exciting the magnetic state of a ferromagnet [122][123].

Magnetization reversal of a ferromagnet can be achieved by applying a spin polarized current. A spin polarized current can be produced by the

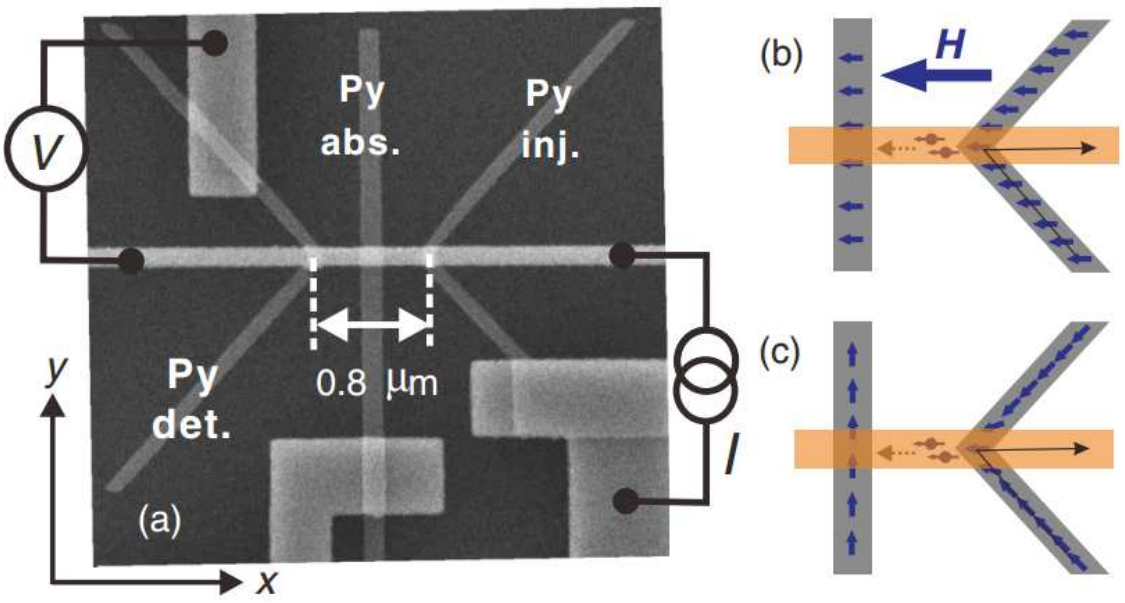

Figure 23. Scanning electron microscope (SEM) image of the specially fabricated Py/Cu lateral spin valve consisting of two V-shaped nanowires with a middle strip. Expected domain structures in the Py wires and spin accumulation in a Cu channel for the longitudinal configuration (b) and the transverse configuration (c). “Reprinted (Figure 1) with permission from [(Nonoguchi, S., T. Nomura, and T. Kimura., Physical Review B, "Longitudinal and transverse spin current absorptions in a lateral spin-valve structure", vol. 86.10, pp. 104417-1 - 104417-5, (2012)) Copyright (2012) by the American Physical Society.” [120].

transmission of an electrical current through a magnetic layer. Switching the magnetization of the detection electrode using pure spin current in lateral spin valves is in great interest recently. A group from Purdue University has demonstrated first spin transfer torque experiment in

graphene assisted by an external magnetic field in a lateral non-local spin valve [32]. Magnetization switching of a 5 nm thin Py electrode defined on a 7 layer thick graphene has been demonstrated with a current pulse of 4.5 mA for 5 μs and with an assisted external magnetic field of 4 mT in plane. Required external magnetic field is further reduced down to 2.5 mT by removing the tunneling barrier underneath the Py electrode [33]. Schematic structure and scanning electron micrograph of the graphene LNLSV device used for spin torque experiments are given in Figure 26.

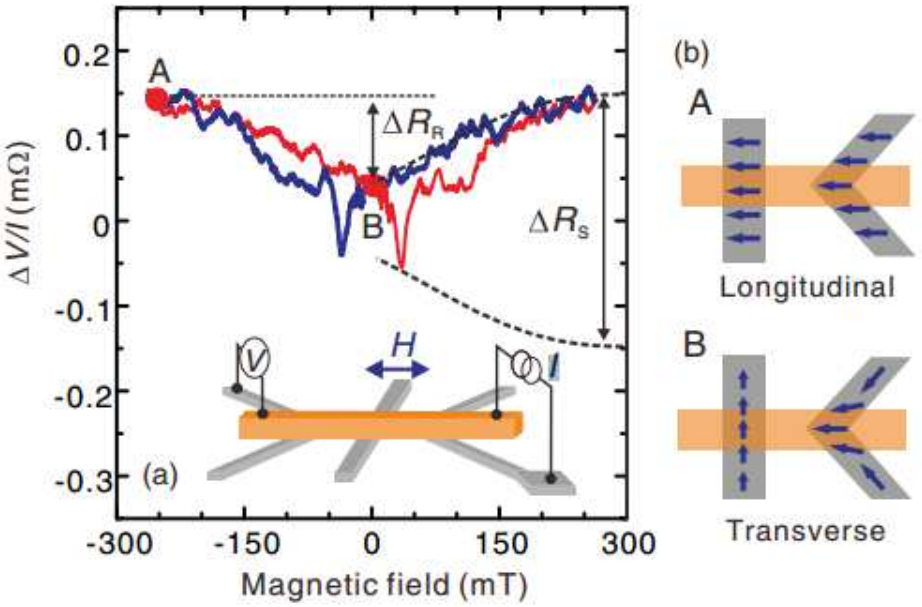

Figure 24. (a) Nonlocal spin valve signal using the V-shaped Py injector and detector with the middle Py absorber under the magnetic field along the x direction (parallel to the Cu strip). (b) Schematic illustrations for the domain structures of the V-shaped injector, detector, and absorber at the fully parallel (A) and the remanent (B) states. “Reprinted (Figure 4) with permission from [(Nonoguchi, S., T. Nomura, and T. Kimura., Physical Review B, "Longitudinal and transverse spin current absorptions in a lateral spin-valve structure", vol. 86.10, pp. 104417-1 - 104417-5, (2012)) Copyright (2012) by the American Physical Society.” [120].

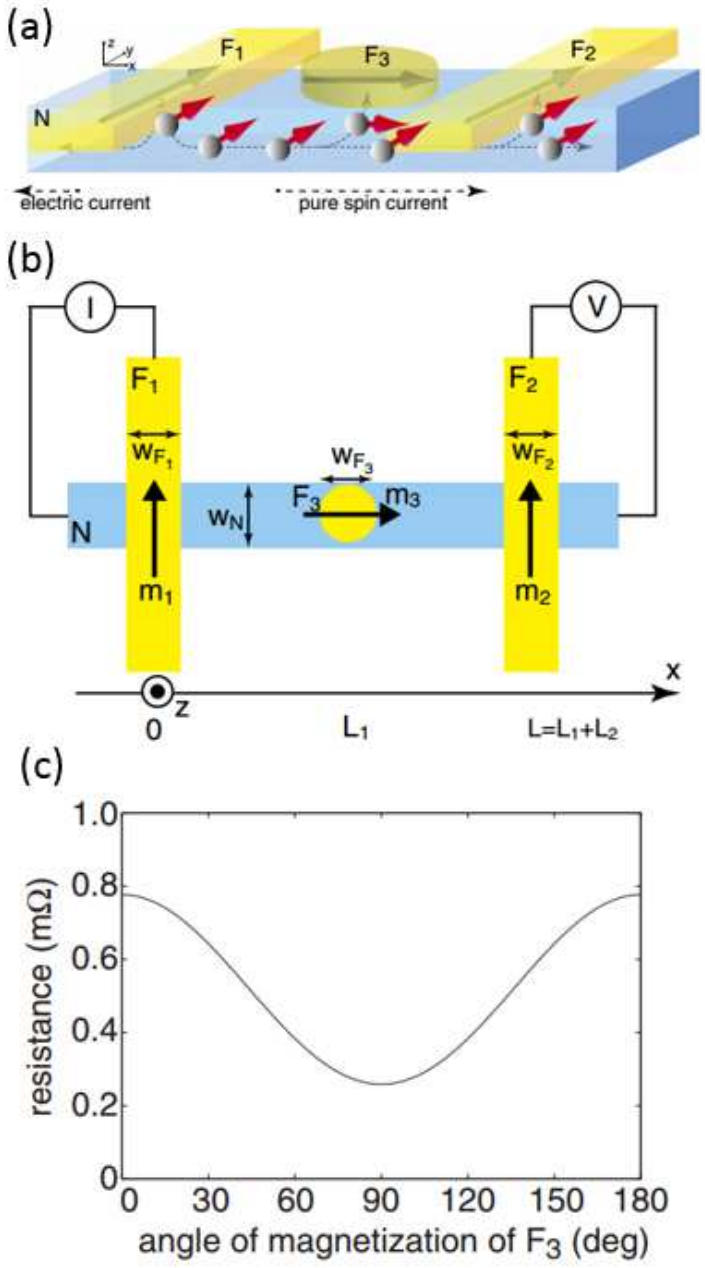

Figure 25. Schematic view of the nonlocal spin valve with three ferromagnetic (F) layer (b) The top view of the system. (c) The dependence of the magnetoresistance on the relative angle between m1 and m3. “Reprinted (Figure 1, Figure 2-a, and Figure 3) from (Taniguchi, Tomohiro, and Hiroshi Imamura., "Proposal of an experimental scheme for determination of penetration depth of transverse spin current by a nonlocal spin valve" Journal of the Physical Society of Japan 81.12 (2012): 124704.)” [121].

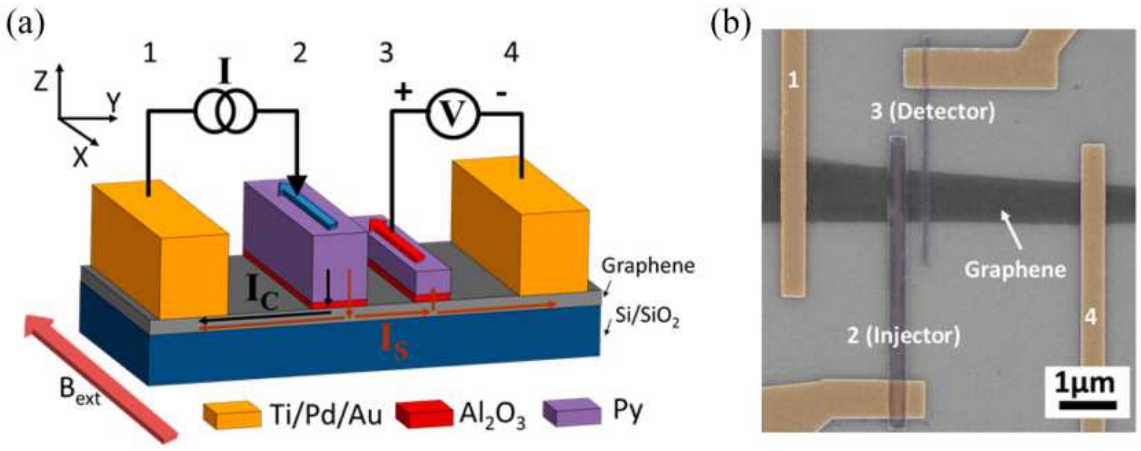

Figure 26. Graphene LNLSV device structure. (a) Schematic structure and (b) scanning electron micrograph of a graphene LNLSV device used for spin torque experiments. “Reprinted (adapted) with permission from (Lin, Chia-Ching, et al. "Spin transfer torque in a graphene lateral spin valve assisted by an external magnetic field." Nano letters 13.11 (2013): 5177-5181.). Copyright (2013) American Chemical Society.” [32].

References

[1] Arns, R.G., 1998. The other transistor: early history of the metal-oxide semiconductor field-effect transistor. *Engineering Science and Education Journal*, *7*(5), pp.233-240.

[2] Deal, B.E. and Early, J.M., 1979. The evolution of silicon semiconductor technology: 1952–1977. *Journal of The Electrochemical Society*, *126*(1), pp.20C-32C.

[3] Schulz, M., 1999. The end of the road for silicon?. *Nature*, *399*(6738), pp.729-730.

[4] Iwai, H., 2009, June. Technology roadmap for 22nm and beyond. In *Electron Devices and Semiconductor Technology, 2009. IEDST'09. 2nd International Workshop on* (pp. 1-4). IEEE.

[5] Mohsenifar, S. and Shahrokhabadi, M.H., 2015. Gate Stack High-κ Materials for Si-Based MOSFETs Past, Present, and Futures. *Microelectronics and Solid State Electronics*, *4*(1), pp.12-24.

[6] Robertson, J. and Wallace, R.M., 2015. High-K materials and metal gates for CMOS applications. *Materials Science and Engineering: R: Reports*, *88*, pp.1-41.

[7] Schwierz, F., Pezoldt, J. and Granzner, R., 2015. Two-dimensional materials and their prospects in transistor electronics. *Nanoscale*, *7*(18), pp.8261-8283.

[8] Adan, A.O. and Higashi, K., 2001. OFF-State leakage current mechanisms in bulkSi and SOI MOSFETs and their impact on CMOS ULSIs standby current.*Electron Devices, IEEE Transactions on*, *48*(9), pp.2050-2057.

[9] Ferain, I., Colinge, C.A. and Colinge, J.P., 2011. Multigate transistors as the future of classical metal-oxide-semiconductor field-effect transistors. *Nature*,*479*(7373), pp.310-316.

[10] Hur, Ibrahim, and Calvin Lin. "A comprehensive approach to DRAM power management." *High Performance Computer Architecture, 2008. HPCA 2008. IEEE 14th International Symposium on*. IEEE, 2008.

[11] Zhang, K., Bhattacharya, U., Chen, Z., Hamzaoglu, F., Murray, D., Vallepalli, N., Wang, Y., Zheng, B. and Bohr, M., 2006. A 3-GHz 70-Mb SRAM in 65-nm CMOS technology with integrated column-based dynamic power supply.*Solid-State Circuits, IEEE Journal of*, *41*(1), pp.146-151.

[12] https://en.wikipedia.org/wiki/Static_random-access_memory#/media/File:SRAM_Cell_(6_Transistors).svg

[13] Meena, J.S., Sze, S.M., Chand, U. and Tseng, T.Y., 2014. Overview of emerging nonvolatile memory technologies. *Nanoscale research letters*, *9*(1), pp.1-33.

[14] Perez, T. and De Rose, C.A., 2010. Non-volatile memory: Emerging technologies and their impacts on memory systems. *Porto Alegre*.

[15] Raoux, S., Burr, G.W., Breitwisch, M.J., Rettner, C.T., Chen, Y.C., Shelby, R.M., Salinga, M., Krebs, D., Chen, S.H., Lung, H.L. and Lam, C.H., 2008. Phase-change random access memory: A scalable technology. *IBM Journal of Research and Development*, *52*(4.5), pp.465-479.

[16] Ma, T.P. and Han, J.P., 2002. Why is nonvolatile ferroelectric memory field-effect transistor still elusive?. *Electron Device Letters, IEEE*, *23*(7), pp.386-388.

[17] Guillaume, P.R.E.N.A.T., Jabeur, K., Vanhauwaert, P., Pendina, G., Oboril, F., Bishnoi, R., Garello, K., Gambardella, P., Tahoori, M. and Gaudin, G., Ultra-Fast and High-Reliability SOT-MRAM: from Cache Replacement to Normally-off Computing.

[18] Parkin, S.S., Hayashi, M. and Thomas, L., 2008. Magnetic domain-wall racetrack memory. *Science*, *320*(5873), pp.190-194.

[19] Baibich, M.N., Broto, J.M., Fert, A., Van Dau, F.N., Petroff, F., Etienne, P., Creuzet, G., Friederich, A. and Chazelas, J., 1988. Giant magnetoresistance of (001) Fe/(001) Cr magnetic superlattices. *Physical review letters*, *61*(21), p.2472.

[20] Binasch, G., Grünberg, P., Saurenbach, F. and Zinn, W., 1989. Enhanced magnetoresistance in layered magnetic structures with

antiferromagnetic interlayer exchange. *Physical review B*, *39*(7), p.4828.

[21] Takagishi, M., Yoshikawa, M., Funayama, T., Iwasaki, H. and Sahashi, M., 2002. The applicability of CPP-GMR heads for magnetic recording.*Magnetics, IEEE Transactions on*, *38*(5), pp.2277-2282.

[22] Daughton, J.M. and Chen, Y.J., 1993. GMR materials for low field applications. *Magnetics, IEEE Transactions on*, *29*(6), pp.2705-2710.

[23] Rottmayer, R. and Zhu, J.G., 1995. A new design for an ultra-high density magnetic recording head using a GMR sensor in the CPP mode. *Magnetics, IEEE Transactions on*, *31*(6), pp.2597-2599.

[24] Park, B.G., Wunderlich, J., Martí, X., Holý, V., Kurosaki, Y., Yamada, M., Yamamoto, H., Nishide, A., Hayakawa, J., Takahashi, H. and Shick, A.B., 2011. A spin-valve-like magnetoresistance of an antiferromagnet-based tunnel junction. *Nature materials*, *10*(5), pp.347-351.

[25] Daughton, J.M., 1999. GMR applications. *Journal of Magnetism and Magnetic Materials*, *192*(2), pp.334-342.

[26] Wang, K.L., Alzate, J.G. and Amiri, P.K., 2013. Low-power non-volatile spintronic memory: STT-RAM and beyond. *Journal of Physics D: Applied Physics*, *46*(7), p.074003.

[27] Chen, E., Apalkov, D., Diao, Z., Driskill-Smith, A., Druist, D., Lottis, D., Nikitin, V., Tang, X., Watts, S., Wang, S. and Wolf, S.A., 2010. Advances and future prospects of spin-transfer torque random access memory. *Magnetics, IEEE Transactions on*, *46*(6), pp.1873-1878.

[28] Park, B.G., Wunderlich, J., Martí, X., Holý, V., Kurosaki, Y., Yamada, M., Yamamoto, H., Nishide, A., Hayakawa, J., Takahashi, H. and Shick, A.B., 2011. A spin-valve-like magnetoresistance of an antiferromagnet-based tunnel junction. *Nature materials*, *10*(5), pp.347-351.

[29] Li, Z. and Zhang, S., 2003. Magnetization dynamics with a spin-transfer torque. *Physical Review B*, *68*(2), p.024404.

[30] Cho, S., Chen, Y.F. and Fuhrer, M.S., 2007. Gate-tunable graphene spin valve. *Applied Physics Letters*, *91*(12), p.123105.

[31] Lee, D.H. and Lim, S.H., 2008. Increase of temperature due to Joule heating during current-induced magnetization switching of an MgO-based magnetic tunnel junction. *Applied Physics Letters*, *92*(23), p.233502.

[32] Lin, C.C., Penumatcha, A.V., Gao, Y., Diep, V.Q., Appenzeller, J. and Chen, Z., 2013. Spin transfer torque in a graphene lateral spin valve assisted by an external magnetic field. *Nano letters*, *13*(11), pp.5177-5181.

[33] Lin, C.C., Gao, Y., Penumatcha, A.V., Diep, V.Q., Appenzeller, J. and Chen, Z., 2014. Improvement of spin transfer torque in asymmetric graphene devices. *ACS nano*, *8*(4), pp.3807-3812.

[34] Han, W., McCreary, K.M., Pi, K., Wang, W.H., Li, Y., Wen, H., Chen, J.R. and Kawakami, R.K., 2012. Spin transport and relaxation in graphene. *Journal of Magnetism and Magnetic Materials*, *324*(4), pp.369-381.

[35] Chi, P., Li, S., Cheng, Y., Lu, Y., Kang, S.H. and Xie, Y., 2016, January. Architecture design with STT-RAM: Opportunities and challenges. In *2016 21st Asia and South Pacific Design Automation Conference (ASP-DAC)* (pp. 109-114). IEEE.

[36] Chelikowsky, J.R. and Franciosi, A. eds., 2012. *Electronic materials: a new era in materials science* (Vol. 95). Springer Science & Business Media.

[37] Gatos, Harry C. "Semiconductor electronics and the birth of the modern science of surfaces." *Surface science* 299 (1994): 1-23.

[38] Capasso, F., 1987. Materials to New Semiconductor Devices. *Science*, *235*, p.172.

[39] Mas-Balleste, R., Gomez-Navarro, C., Gomez-Herrero, J. and Zamora, F., 2011. 2D materials: to graphene and beyond. *Nanoscale*, *3*(1), pp.20-30.

[40] Gao, Yang, et al. "Elastic coupling between layers in two-dimensional materials." *Nature materials* 14.7 (2015): 714-720.

[41] Gupta, Ankur, Tamilselvan Sakthivel, and Sudipta Seal. "Recent development in 2D materials beyond graphene." *Progress in Materials Science* 73 (2015): 44-126.

[42] Duan, X., Wang, C., Pan, A., Yu, R. and Duan, X., 2015. Two-dimensional transition metal dichalcogenides as atomically thin semiconductors: opportunities and challenges. *Chemical Society Reviews*, *44*(24), pp.8859-8876.

[43] Cattelan, M., Markman, B., Lucchini, G., Das, P.K., Vobornik, I., Robinson, J.A., Agnoli, S. and Granozzi, G., 2015. New Strategy for the Growth of Complex Heterostructures Based on Different 2D Materials. *Chemistry of Materials*, *27*(11), pp.4105-4113.

[44] Kim, K.S., Zhao, Y., Jang, H., Lee, S.Y., Kim, J.M., Kim, K.S., Ahn, J.H., Kim, P., Choi, J.Y. and Hong, B.H., 2009. Large-scale pattern growth of graphene films for stretchable transparent electrodes. *Nature*, *457*(7230), pp.706-710.

[45] Lu, N., Guo, H., Li, L., Dai, J., Wang, L., Mei, W.N., Wu, X. and Zeng, X.C., 2014. MoS 2/MX 2 heterobilayers: bandgap engineering via tensile strain or external electrical field. *Nanoscale*, *6*(5), pp.2879-2886.

[46] Lezama, I.G., Arora, A., Ubaldini, A., Barreteau, C., Giannini, E., Potemski, M. and Morpurgo, A.F., 2015. Indirect-to-direct band gap crossover in few-layer MoTe2. *Nano letters*, *15*(4), pp.2336-2342.

[47] Geim, A.K. and Novoselov, K.S., 2007. The rise of graphene. *Nature materials*, *6*(3), pp.183-191.

[48] Bunch, J.S., Van Der Zande, A.M., Verbridge, S.S., Frank, I.W., Tanenbaum, D.M., Parpia, J.M., Craighead, H.G. and McEuen, P.L., 2007. Electromechanical resonators from graphene sheets. *Science*, *315*(5811), pp.490-493.

[49] Gray, A., Balooch, M., Allegret, S., De Gendt, S. and Wang, W.E., 2008. Optical detection and characterization of graphene by

broadband spectrophotometry. *Journal of Applied Physics*, *104*(5), p.053109.

[50] Blake, P., Hill, E.W., Neto, A.C., Novoselov, K.S., Jiang, D., Yang, R., Booth, T.J. and Geim, A.K., 2007. Making graphene visible. *Applied Physics Letters*,*91*(6), p.063124.

[51] Huang, Y., Dong, X., Shi, Y., Li, C.M., Li, L.J. and Chen, P., 2010. Nanoelectronic biosensors based on CVD grown graphene. *Nanoscale*, *2*(8), pp.1485-1488.

[52] Neto, A.C., Guinea, F., Peres, N.M.R., Novoselov, K.S. and Geim, A.K., 2009. The electronic properties of graphene. *Reviews of modern physics*,*81*(1), p.109.

[53] Chen, J.H., Jang, C., Xiao, S., Ishigami, M. and Fuhrer, M.S., 2008. Intrinsic and extrinsic performance limits of graphene devices on SiO2. *Nature nanotechnology*, *3*(4), pp.206-209.

[54] Bolotin, K.I., Sikes, K.J., Jiang, Z., Klima, M., Fudenberg, G., Hone, J., Kim, P. and Stormer, H.L., 2008. Ultrahigh electron mobility in suspended graphene. *Solid State Communications*, *146*(9), pp.351-355.

[55] Liu, G., Velasco Jr, J., Bao, W. and Lau, C.N., 2008. Fabrication of graphene pnp junctions with contactless top gates. *Applied Physics Letters*, *92*(20), p.203103.

[56] Traversi, F., Russo, V. and Sordan, R., 2009. Integrated complementary graphene inverter. *arXiv preprint arXiv:0904.2745*.

[57] Xia, F., Farmer, D.B., Lin, Y.M. and Avouris, P., 2010. Graphene field-effect transistors with high on/off current ratio and large transport band gap at room temperature. *Nano letters*, *10*(2), pp.715-718.

[58] Fiori, G., Neumaier, D., Szafranek, B.N. and Iannaccone, G., 2014. Bilayer graphene transistors for analog electronics. *Electron Devices, IEEE Transactions on*, *61*(3), pp.729-733.

[59] Bai, J., Zhong, X., Jiang, S., Huang, Y. and Duan, X., 2010. Graphene nanomesh. *Nature nanotechnology*, *5*(3), pp.190-194.

[60] Joensen, P., Frindt, R.F. and Morrison, S.R., 1986. Single-layer MoS 2.*Materials research bulletin*, *21*(4), pp.457-461.

[61] Late, D.J., Liu, B., Matte, H.R., Dravid, V.P. and Rao, C.N.R., 2012. Hysteresis in single-layer MoS2 field effect transistors. *Acs Nano*, *6*(6), pp.5635-5641.

[62] Mak, K.F., Lee, C., Hone, J., Shan, J. and Heinz, T.F., 2010. Atomically thin MoS 2: a new direct-gap semiconductor. *Physical Review Letters*, *105*(13), p.136805.

[63] Bertolazzi, S., Krasnozhon, D. and Kis, A., 2013. Nonvolatile memory cells based on MoS2/graphene heterostructures. *Acs Nano*, *7*(4), pp.3246-3252.

[64] Perkins, F.K., Friedman, A.L., Cobas, E., Campbell, P.M., Jernigan, G.G. and Jonker, B.T., 2013. Chemical vapor sensing with monolayer MoS2. *Nano letters*, *13*(2), pp.668-673.

[65] Radisavljevic, B., Radenovic, A., Brivio, J., Giacometti, V. and Kis, A., 2011. Single-layer MoS2 transistors. *Nature nanotechnology*, *6*(3), pp.147-150.

[66] Radisavljevic, B., Whitwick, M.B. and Kis, A., 2011. Integrated circuits and logic operations based on single-layer MoS2. *ACS nano*, *5*(12), pp.9934-9938.

[67] Fang, H., Chuang, S., Chang, T.C., Takei, K., Takahashi, T. and Javey, A., 2012. High-performance single layered WSe2 p-FETs with chemically doped contacts. *Nano letters*, *12*(7), pp.3788-3792.

[68] Ohno, H., 2001. Toward functional spintronics. *Science*, *291*(5505), pp.840-841.

[69] Wolf, S.A., Lu, J., Stan, M.R., Chen, E. and Treger, D.M., 2010. The promise of nanomagnetics and spintronics for future logic and universal memory.*Proceedings of the IEEE*, *98*(12), pp.2155-2168.

[70] Fert, A., 2008. The present and the future of spintronics. *Thin Solid Films*,*517*(1), pp.2-5.

[71] Baibich, M.N., Broto, J.M., Fert, A., Van Dau, F.N., Petroff, F., Etienne, P., Creuzet, G., Friederich, A. and Chazelas, J., 1988. Giant magnetoresistance of (001) Fe/(001) Cr magnetic superlattices. *Physical review letters*, *61*(21), p.2472.

[72] Binasch, G., Grünberg, P., Saurenbach, F. and Zinn, W., 1989. Enhanced magnetoresistance in layered magnetic structures with antiferromagnetic interlayer exchange. *Physical review B*, *39*(7), p.4828.

[73] Awschalom, D.D., Flatté, M.E. and Samarth, N., 2002. Spintronics. *Scientific American*, *286*(6), pp.66-73.

[74] Žutić, I., Fabian, J. and Sarma, S.D., 2004. Spintronics: Fundamentals and applications. *Reviews of modern physics*, *76*(2), p.323.

[75] Chappert, C., Fert, A. and Van Dau, F.N., 2007. The emergence of spin electronics in data storage. *Nature materials*, *6*(11), pp.813-823.

[76] Verschuur, G.L., 1993. *Hidden Attraction: The History and Mystery of Magnetism: The History and Mystery of Magnetism*. Oxford University Press, USA.

[77] Blundell, S.J., 2012. *Magnetism: A very short introduction*. OUP Oxford.

[78] Stöhr, J. and Siegmann, H.C., 2006. Magnetism. *Solid-State Sciences. Springer, Berlin, Heidelberg*, *5*.

[79] Awschalom, D.D. and Kikkawa, J.M., 1999. Electron spin and optical coherence in semiconductors. *Physics Today*, *52*, pp.33-39.

[80] General Chemistry, 3rd edition, by Hill and Petrucci and Electricity and Magnetism: Berkeley Physics Course," Vol. 2, 2nd ed., by Edward M. Purcell

[81] Shen, X., Sun, L., Yi, Z., Benassi, E., Zhang, R., Shen, Z., Sanvito, S. and Hou, S., 2010. Spin transport properties of 3d transition metal (II) phthalocyanines in contact with single-walled carbon nanotube

electrodes.*Physical Chemistry Chemical Physics*, *12*(36), pp.10805-10811.

[82] Tsukagoshi, K., Alphenaar, B.W. and Ago, H., 1999. Coherent transport of electron spin in a ferromagnetically contacted carbon nanotube. *Nature*,*401*(6753), pp.572-574.

[83] Wolf, S.A., Awschalom, D.D., Buhrman, R.A., Daughton, J.M., Von Molnar, S., Roukes, M.L., Chtchelkanova, A.Y. and Treger, D.M., 2001. Spintronics: a spin-based electronics vision for the future. *Science*, *294*(5546), pp.1488-1495.

[84] Fert, A., 2008. Nobel lecture: Origin, development, and future of spintronics.*Reviews of Modern Physics*, *80*(4), p.1517.

[85] Jedema, F.J., Filip, A.T. and Van Wees, B.J., 2001. Electrical spin injection and accumulation at room temperature in an all-metal mesoscopic spin valve.*Nature*, *410*(6826), pp.345-348.

[86] Jedema, F.J., Heersche, H.B., Filip, A.T., Baselmans, J.J.A. and Van Wees, B.J., 2002. Electrical detection of spin precession in a metallic mesoscopic spin valve. *Nature*, *416*(6882), pp.713-716.

[87] Bruno, P. and Chappert, C., 1991. Oscillatory coupling between ferromagnetic layers separated by a nonmagnetic metal spacer. *Physical Review Letters*, *67*(12), p.1602.

[88] Nickel, J., 1995. *Magnetoresistance overview*. Palo Alto, CA, USA: Hewlett-Packard Laboratories, Technical Publications Department.

[89] Hütten, A., Mrozek, S., Heitmann, S., Hempel, T., Brückl, H. and Reiss, G., 1999. Evolution of the GMR-effect amplitude in copper/permalloy-multilayered thin films. *Acta materialia*, *47*(15), pp.4245-4252.

[90] Prinz, G.A., 1998. Magnetoelectronics. *Science*, *282*(5394), pp.1660-1663.

[91] Obeid, S. and Dogaru, T., 2015, April. Improvement on printed circuit board inspection using injected AC current and GMR magnetic sensor. In*Technological Advances in Electrical, Electronics and*

Computer Engineering (TAEECE), 2015 Third International Conference on (pp. 150-154). IEEE.

[92] Freitas, P.P., Silva, F., Oliveira, N.J., Melo, L.V., Costa, L. and Almeida, N., 2000. Spin valve sensors. *Sensors and Actuators A: Physical*, *81*(1), pp.2-8.

[93] Dieny, B., 1994. Giant magnetoresistance in spin-valve multilayers. *Journal of Magnetism and Magnetic Materials*, *136*(3), pp.335-359.

[94] Felser, C., Fecher, G.H. and Balke, B., 2007. Spintronics: a challenge for materials science and solid-state chemistry. *Angewandte Chemie International Edition*, *46*(5), pp.668-699.

[95] Pershin, Y.V. and Di Ventra, M., 2008. Spin memristive systems: Spin memory effects in semiconductor spintronics. *Physical Review B*, *78*(11), p.113309.

[96] Jin, K.X., Zhao, S.G. and Chen, C.L., 2009. Transport characteristic in current-in-plane (CIP) geometry of La 0.8 Sr 0.2 MnO 3/Co heterostructure.*Physica B: Condensed Matter*, *404*(8), pp.1515-1517.

[97] Bass, J., 2013. Current perpendicular-to-plane (CPP) magnetoresistance (MR). *arXiv preprint arXiv:1305.3848*.

[98] Gopinadhan, K., Shin, Y.J., Jalil, R., Venkatesan, T., Geim, A.K., Neto, A.H.C. and Yang, H., 2015. Extremely large magnetoresistance in few-layer graphene/boron-nitride heterostructures. *Nature communications*, *6*.

[99] Tombros, N., Jozsa, C., Popinciuc, M., Jonkman, H.T. and Van Wees, B.J., 2007. Electronic spin transport and spin precession in single graphene layers at room temperature. *Nature*, *448*(7153), pp.571-574.

[100] Appelbaum, I., Huang, B. and Monsma, D.J., 2007. Electronic measurement and control of spin transport in silicon. *Nature*, *447*(7142), pp.295-298.

[101] Lou, X., Adelmann, C., Crooker, S.A., Garlid, E.S., Zhang, J., Reddy, K.M., Flexner, S.D., Palmstrøm, C.J. and Crowell, P.A., 2007. Electrical detection of spin transport in lateral ferromagnet–semiconductor devices. *Nature Physics*, *3*(3), pp.197-202.

[102] Zhang, X., Mizukami, S., Kubota, T., Ma, Q., Oogane, M., Naganuma, H., Ando, Y. and Miyazaki, T., 2013. Observation of a large spin-dependent transport length in organic spin valves at room temperature. *Nature communications*, *4*, p.1392.

[103] Meng, J., Chen, J.J., Yan, Y., Yu, D.P. and Liao, Z.M., 2013. Vertical graphene spin valve with Ohmic contacts. *Nanoscale*, *5*(19), pp.8894-8898.

[104] Han, W., McCreary, K.M., Pi, K., Wang, W.H., Li, Y., Wen, H., Chen, J.R. and Kawakami, R.K., 2012. Spin transport and relaxation in graphene. *Journal of Magnetism and Magnetic Materials*, *324*(4), pp.369-381.

[105] Shklovskii, B.I., 2006. Dyakonov-Perel spin relaxation near the metal-insulator transition and in hopping transport. *Physical Review B*, *73*(19), p.193201.

[106] Kiss, A., Szolnoki, L. and Simon, F., 2015. The Elliott-Yafet theory of spin relaxation generalized for large spin-orbit coupling. *arXiv preprint arXiv:1512.03204*.

[107] Bir, G.L., Aronov, A.G. and Pikus, G.E., 1976. Spin relaxation of electrons due to scattering by holes. *Soviet Journal of Experimental and Theoretical Physics*, *42*, p.705.

[108] Johnson, M. and Silsbee, R.H., 1985. Interfacial charge-spin coupling: Injection and detection of spin magnetization in metals. *Physical Review Letters*, *55*(17), p.1790.

[109] Kikkawa, J.M. and Awschalom, D.D., 1999. Lateral drag of spin coherence in gallium arsenide. *Nature*, *397*(6715), pp.139-141.

[110] Schmidt, G., Ferrand, D., Molenkamp, L.W., Filip, A.T. and Van Wees, B.J., 2000. Fundamental obstacle for electrical spin injection from a ferromagnetic metal into a diffusive semiconductor. *Physical Review B*, *62*(8), p.R4790.

[111] Rashba, E.I., 2000. Theory of electrical spin injection: Tunnel contacts as a solution of the conductivity mismatch problem. *Physical Review B*, *62*(24), p.R16267.

[112] Lou, X., Adelmann, C., Crooker, S.A., Garlid, E.S., Zhang, J., Reddy, K.M., Flexner, S.D., Palmstrøm, C.J. and Crowell, P.A., 2007. Electrical detection of spin transport in lateral ferromagnet–semiconductor devices. *Nature Physics*, *3*(3), pp.197-202.

[113] Appelbaum, I., Huang, B. and Monsma, D.J., 2007. Electronic measurement and control of spin transport in silicon. *Nature*, *447*(7142), pp.295-298.

[114] Bass, J. and Pratt Jr, W.P., 2007. Spin-diffusion lengths in metals and alloys, and spin-flipping at metal/metal interfaces: an experimentalist's critical review.*Journal of Physics: Condensed Matter*, *19*(18), p.183201.

[115] Huertas-Hernando, D., Guinea, F. and Brataas, A., 2006. Spin-orbit coupling in curved graphene, fullerenes, nanotubes, and nanotube caps. *Physical Review B*, *74*(15), p.155426.

[116] Han, W., Kawakami, R.K., Gmitra, M. and Fabian, J., 2014. Graphene spintronics. *Nature nanotechnology*, *9*(10), pp.794-807.

[117] Han, W., Pi, K., McCreary, K.M., Li, Y., Wong, J.J., Swartz, A.G. and Kawakami, R.K., 2010. Tunneling spin injection into single layer graphene.*Physical review letters*, *105*(16), p.167202.

[118] Han, W. and Kawakami, R.K., 2011. Spin relaxation in single-layer and bilayer graphene. *Physical review letters*, *107*(4), p.047207.

[119] Dlubak, B., Martin, M.B., Deranlot, C., Servet, B., Xavier, S., Mattana, R., Sprinkle, M., Berger, C., De Heer, W.A., Petroff, F. and Anane, A., 2012. Highly efficient spin transport in epitaxial graphene on SiC. *Nature Physics*,*8*(7), pp.557-561.

[120] Nonoguchi, S., Nomura, T. and Kimura, T., 2012. Longitudinal and transverse spin current absorptions in a lateral spin-valve structure. *Physical Review B*,*86*(10), p.104417.

[121] Taniguchi, T. and Imamura, H., 2012. Proposal of an experimental scheme for determination of penetration depth of transverse spin current by a nonlocal spin valve. *Journal of the Physical Society of Japan*, *81*(12), p.124704.

[122] Slonczewski, J.C., 1999. Excitation of spin waves by an electric current. *Journal of Magnetism and Magnetic Materials*, *195*(2), pp.L261-L268.

[123] Berger, L., 1996. Emission of spin waves by a magnetic multilayer traversed by a current. *Physical Review B*, *54*(13), p.9353.

Chapter 2

2.1 Characterization of MoS_2 and FET Fabrication

Field effect transistors (FETs) have been fabricated to characterize exfoliated/CVD grown MoS_2 films. The following chapter presents the experimental results based on the FETs fabricated using MoS_2 films.

2.2 Top gate FETs on Exfoliated and CVD grown MoS_2 film

This section presents the experimental results for the characterization of exfoliated and CVD grown MoS_2 with top gate FETs. Design parameters have been selected as 40 nm for the dielectric thickness and 6 μm as the channel length.

Prior to fabrication, exfoliated and CVD grown MoS_2 films have been characterized by atomic force microscopy and Raman spectroscopy. The existence of the MoS_2 film was confirmed using Raman spectroscopy while the thickness measurements were done using AFM. Raman peaks of the exfoliated MoS_2 film exhibit a bulk behavior which is also verified by AFM measurements while CVD grown MoS_2 film exhibits a monolayer behavior. Schematic of the CVD grown MoS_2 top gate field effect transistor and optical micrograph (upper right) of the device is shown in Figure 27. The device is fabricated on a Si substrate covered with a 300 nm SiO_2 layer. The source and drain contacts are defined by electron beam lithography

and consist of Ti/Au (10/80 nm) metals while HfO_2 is used as the dielectric owing to its perfect insulating and high k dielectric properties. Detailed fabrication process is given in Appendix A and Appendix B.

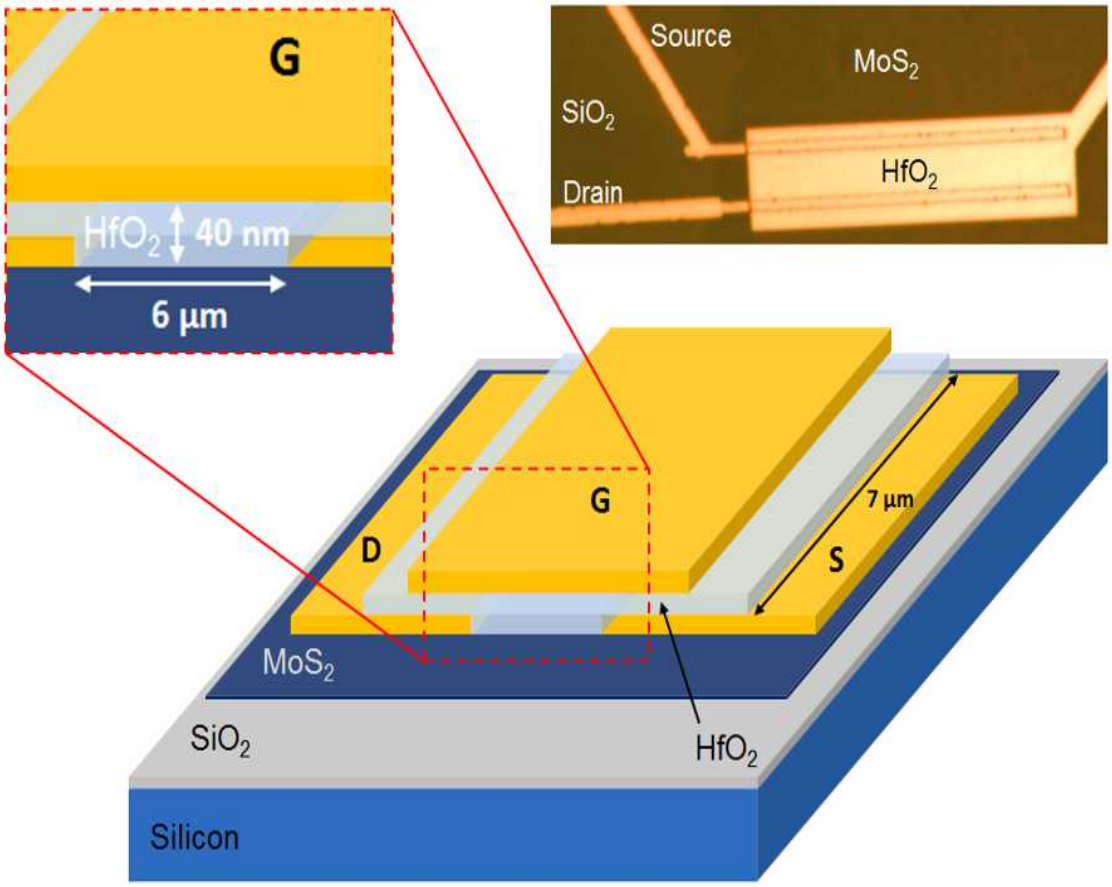

Figure 27. Schematic of the CVD grown MoS_2 top gate field effect transistor and optical micrograph of the MoS_2 device (upper right).

I_{DS}-V_{DS} and I_{DS}-V_{GS} curves are shown for exfoliated and CVD grown MoS_2 film in Figure 28 and Figure 29, respectively, with 40 nm HfO_2 and channel length of 6 µm. I_{DS}-V_{DS} curves are recorded for different values of V_{GS}. I_{DS}-V_{GS} curves are plotted for a bias voltage ranging from 50 mV to 500 mV.

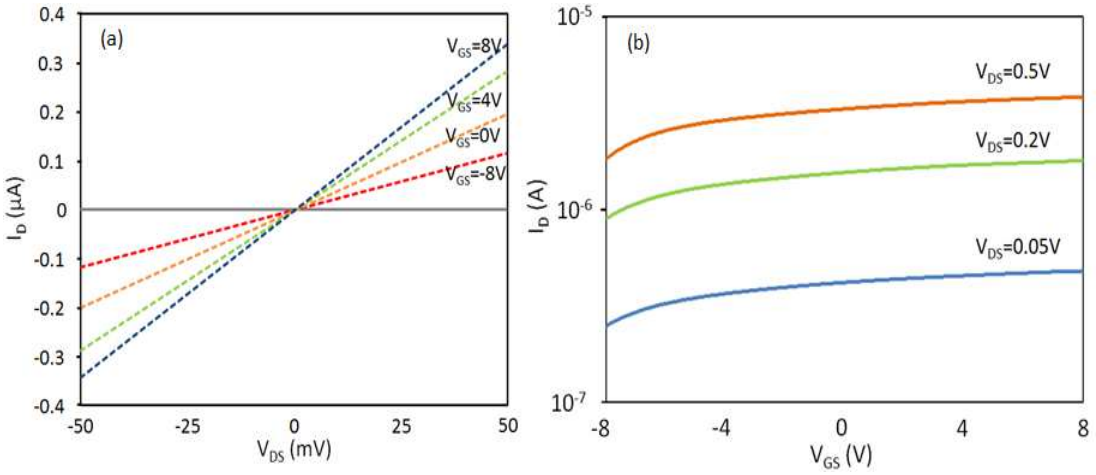

Figure 28. (a) I_{DS}-V_{DS} curves recorded for different values of V_{GS}, for exfoliated MoS_2 (b) I_{DS}-V_{GS} curves recorded for a bias voltage ranging from 50 mV to 500 mV where channel width is 7 μm, channel length is 6 μm and HfO_2 thickness is 40 nm, for exfoliated MoS_2.

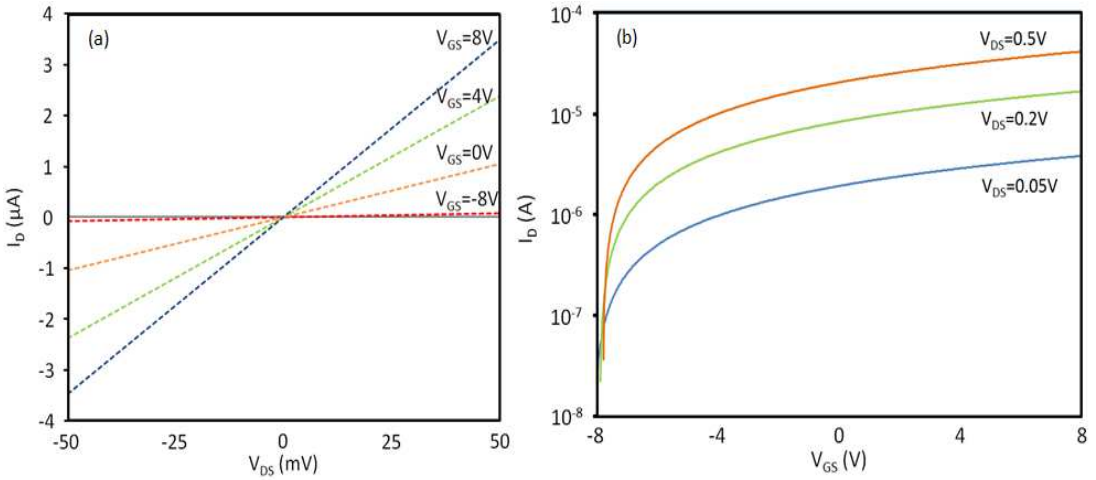

Figure 29. (a) I_{DS}-V_{DS} curves recorded for different values of V_{GS}, for CVD MoS_2 (b) I_{DS}-V_{GS} curves recorded for a bias voltage ranging from 50 mV to 500 mV where channel width is 7 μm, channel length is 6 μm and HfO_2 thickness is 40 nm, for CVD MoS_2.

Exfoliated and CVD grown MoS_2 film are compared in Figure 30. CVD

MoS_2 shows better characteristics with respect to the exfoliated MoS_2,

noting that monolayer CVD MoS_2 film is compared with exfoliated bulk layer MoS_2 film.

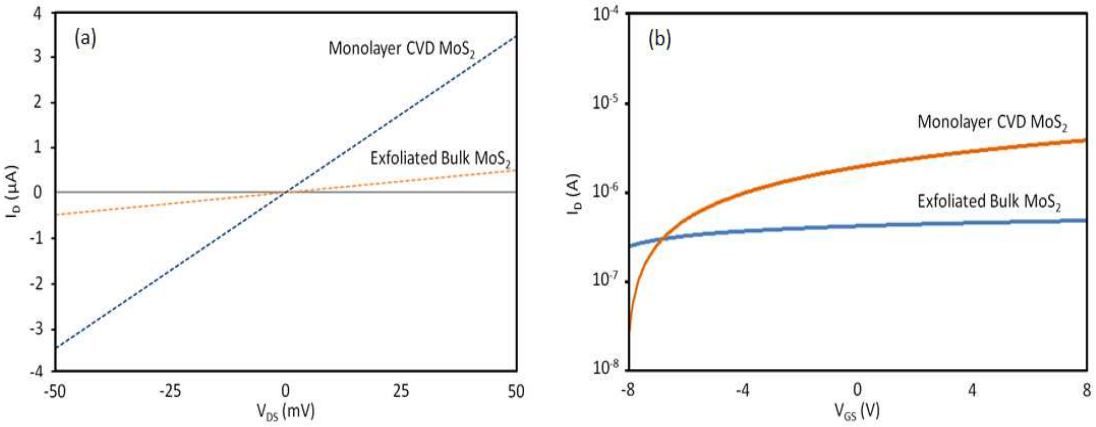

Figure 30. (a) I_{DS}-V_{DS} curves recorded for exfoliated and CVD MoS_2, for different values of V_{GS} (b) I_{DS}-V_{GS} curves recorded for exfoliated and CVD MoS_2 with a bias voltage of 50 mV where channel width is 7 μm, channel length is 6 μm and HfO_2 thickness is 40 nm.

Chapter 3

3.1 Spin absorption in graphene

Spintronic devices are very promising for future information storage/processing and have the potential to replace current CMOS devices. Low energy magnetization switching of a nanomagnet using pure spin current is a key toward all spin logic devices. Graphene constitutes an ideal spin channel material due its high spin diffusion length and long spin lifetime [1][2][3][4]. Furthermore, graphene has high carrier mobility and tunable carrier concentration providing a very unique platform toward low energy spin transfer torque switching [5]. Here, we study spin absorption by a Py nanomagnet grown on top of a lateral graphene spin valve channel. A pure spin current is injected into a graphene channel via electrical spin injection through a Co/Al_2O_3 tunnel barrier junction. The Py island in between the injector and the detector is expected to modulate the spin population at the detector via spin absorption. Depending on the magnetization of the Py island, the spin current can be absorbed differently resulting in a distinct signature of non-local magnetoresistance and hence a modulation of the spin population. We attribute this effect to a combination of both transverse and longitudinal spin current absorptions which is caused by the micro domain formations within the Permalloy island and hence a hysteretic behavior in the MR signal. This

hysteretic behavior can be due to the magnetization rotation of micro domains which raise the discussion of both lateral and longitudinal spin absorption. This new effect is still being investigated and further studies are underway to unravel the origin of this new effect observed in graphene spin valves.

As discussed in the previous chapter, lateral spin valve is basically composed of the spin channel material for spin transport, tunnel barrier for overcoming the conductivity mismatch problem and ferromagnetic electrodes for spin injection and detection. Here, we use graphene as a spin channel material, Al_2O_3 as the tunnel barrier, Co as the ferromagnetic electrodes and Permalloy as the spin absorber. The width, length and thickness of the Permalloy island is 0.5 μm, 1.9 μm and 20 nm, respectively while the graphene channel width is 5 μm. Permalloy island with transparent contact is directly deposited on graphene for efficient spin absorption. Spins are injected from a Co/Al_2O_3 tunnel barrier junction and diffuse towards the detection electrode. The Permalloy island is expected to modulate the spin current distribution in the channel and hence a change in the spin accumulation at the detector due to spin absorption which results in a distinct signature in the MR signal. Depending on the magnetization of the Py island, the spin current can be absorbed differently resulting in a distinct signature of non-local magnetoresistance and hence a modulation of the spin population. We

attribute this effect to a combination of both transverse and longitudinal spin current absorptions which is caused by the micro domain formations within the Permalloy island. This is reflected as a gradual decrease in the MR signal with the magnetic field and a clear hysteretic jump in the signal due to the magnetization switching of the Py. This hysteretic behavior can be due to the magnetization rotation of micro domains which raise the discussion of both lateral and longitudinal spin absorption simultaneously. Device schematics and optical image is given in Figure 31. Non-local measurements shows a hysteretic behavior which is followed by a further decrease of the spin signal. The spin absorption into the Py island depends on the spin resistance given by:

$Rs = 2\rho\lambda/[(1 - P^2)S]$

where λ is the longitudinal or transverse spin diffusion length, P is the spin polarization of the Py island, ρ is the electrical resistivity and S is the cross sectional area [6]. The spin diffusion length term depends on the relative orientation of the spin polarization of the spin current to the magnetization of the island. This results in a faster spin absorption for transverse spin current as compared to longitudinal as pointed out in [6]. The hysteric behavior shown in Figure 32 can be explained in terms of the change in spin resistance due to longitudinal and transverse spin

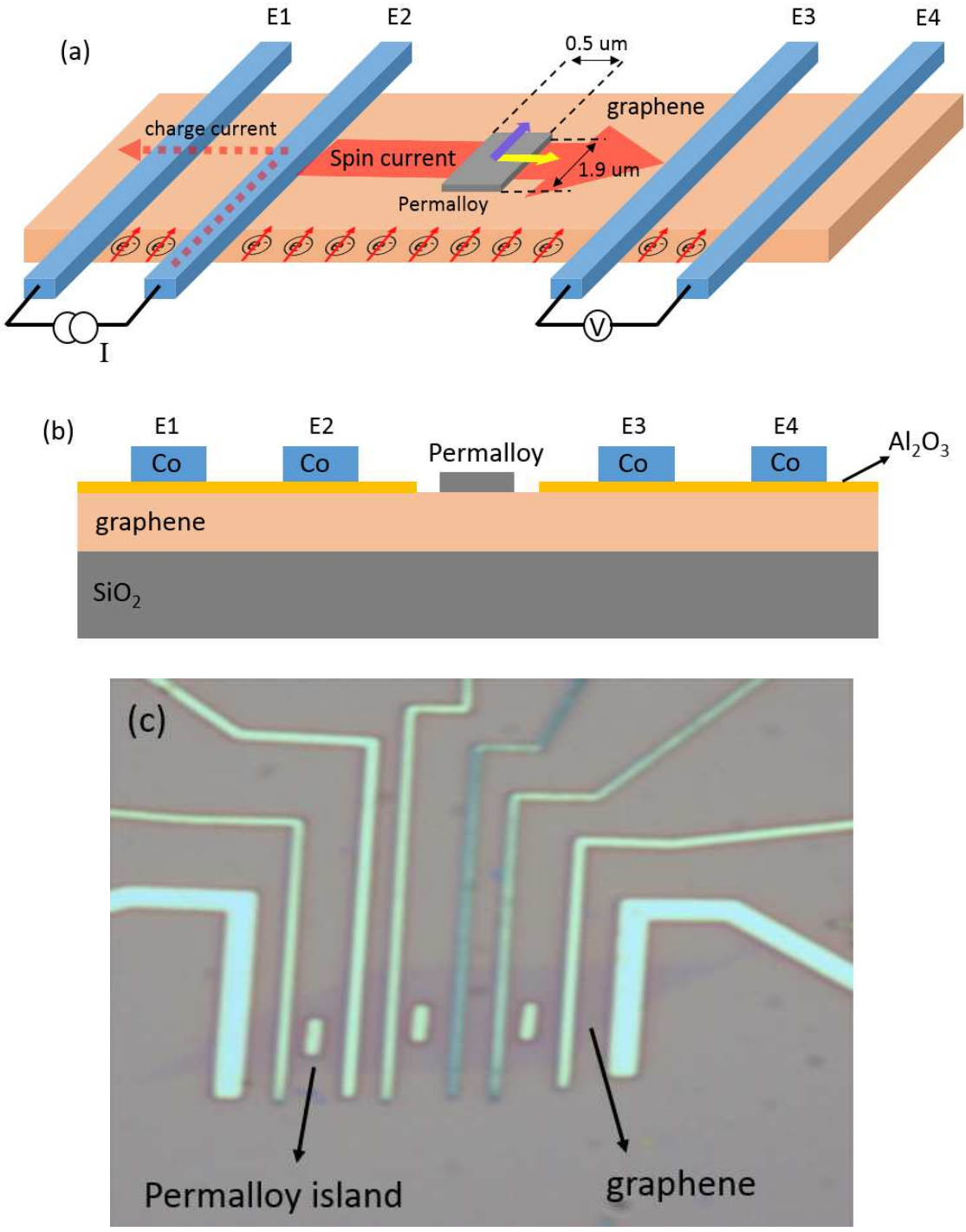

Figure 31. (a-b) Schematic of non-local lateral spin valve with Permalloy island. (c) Optical image of non-local lateral spin valve with Permalloy islands.

absorption happening concurrently due to inhomogeneous magnetization contributions from micro domains within the Permalloy island. Spin absorption can be characterized by the decrease in the MR signal and spin resistance determines the magnitude of the spin absorption. In Figure 32-d, we depict the different states of the Py island as the magnetic field is swept. At point A, the micro domains are aligned with the magnetic field resulting in longitudinal spin absorption. However, as the magnetic field is decreased (point B), the micro domains gradually lose their initial orientation and start aligning transverse to the spin polarization. This results in a decrease of the non-local signal due to the fast spin absorption of the transverse spin current. At positive field (point C), the magnetization is mostly aligned transverse resulting in a further decrease of the spin signal. This transverse anisotropy might be due to the roughness of the interface between the Py island and the graphene which overcomes the shape anisotropy of the island. At point D and E, we observe the main switching of the injector and detector.

It is very important to investigate the anisotropy of the island and correlate the result to the non-local MR measurement. To this end, magnetic force microscopy of the island is needed in order to further confirm the observed non local signal in our devices.

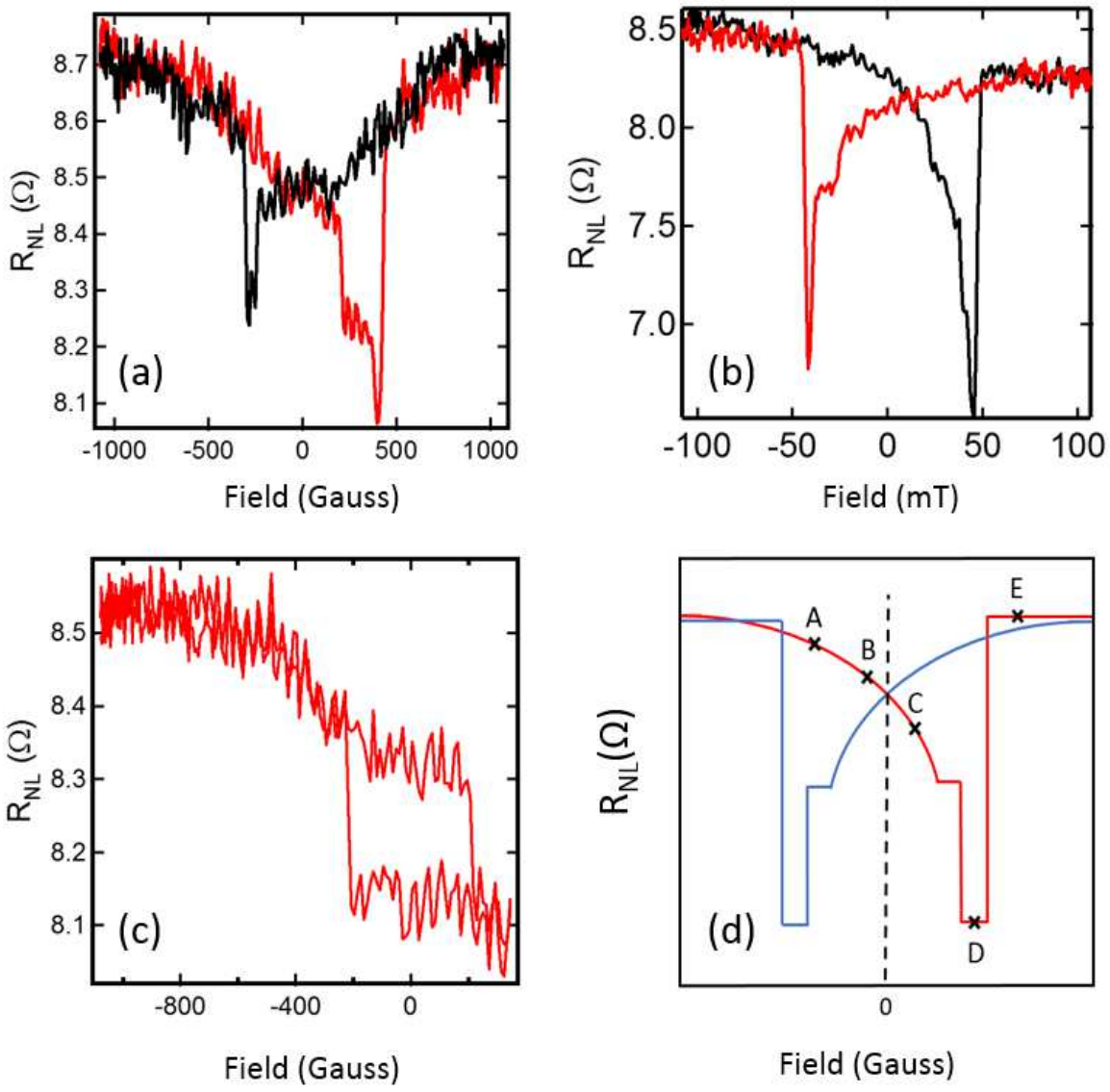

Figure 32. (a-b) Non-local MR measurement (c) Minor loop (d) MR signal schematic for analysis.

Fabrication of the device starts with the exfoliation of graphene on a SiO_2 wafer. Prior to exfoliation, samples are cleaned by ultrasonic cleaning in Acetone and IPA for 10 min and blow dried using nitrogen. This is followed by a heat treatment at 150^{o}C on a hotplate for 30 mins. Exfoliation step

starts with attaching a thin graphite sheet (HOPG) on a scotch tape. This is followed by several folding and peeling steps until thinner layers of graphite obtained on the tape. Graphene is transferred on the wafer by van der Waals forces after detaching the tape [7]. After identifying the graphene on the wafer, electron-beam lithography steps proceed. MMA and PMMA resists are used to ease the lift-off process. Permalloy island is deposited using electron beam evaporation with a thickness of 20 nm and capped with 7 nm Al_2O_3 to prevent further oxidation. This is followed by 0.6 nm Aluminum sputtering and oxidation in the vacuum chamber with oxygen for 30 min to realize Al_2O_3 as a tunnel barrier. Electrodes are patterned with e-beam lithography and Co is deposited using Molecular beam epitaxy with a thickness of 80 nm which was capped with 7 nm Al_2O_3 using e-beam evaporation afterwards.

For the non-local magnetoresistance measurement, a current source is used and 1 μA AC current at 11 Hz is injected through a Co/Al_2O_3 tunnel barrier junction. After spins are injected into graphene, spins tend to diffuse in both directions. Detection electrodes are used to detect the injected spin orientation depending on the magnetization direction of the electrodes. The measured voltage is either positive or negative depending on the relative magnetization orientation of the electrodes.

References

[1] Huertas-Hernando, D., Guinea, F. and Brataas, A., 2006. Spin-orbit coupling in curved graphene, fullerenes, nanotubes, and nanotube caps. *Physical Review B*, *74*(15), p.155426.

[2] Han, W., Kawakami, R.K., Gmitra, M. and Fabian, J., 2014. Graphene spintronics. *Nature nanotechnology*, *9*(10), pp.794-807.

[3] Han, W., Pi, K., McCreary, K.M., Li, Y., Wong, J.J., Swartz, A.G. and Kawakami, R.K., 2010. Tunneling spin injection into single layer graphene.*Physical review letters*, *105*(16), p.167202.

[4] Han, W. and Kawakami, R.K., 2011. Spin relaxation in single-layer and bilayer graphene. *Physical review letters*, *107*(4), p.047207.

[5] Lin, C.C., Penumatcha, A.V., Gao, Y., Diep, V.Q., Appenzeller, J. and Chen, Z., 2013. Spin transfer torque in a graphene lateral spin valve assisted by an external magnetic field. *Nano letters*, *13*(11), pp.5177-5181.

[6] Nonoguchi, S., Nomura, T. and Kimura, T., 2012. Longitudinal and transverse spin current absorptions in a lateral spin-valve structure. *Physical Review B*,*86*(10), p.104417.

[7] Lee, C., Wei, X., Kysar, J.W. and Hone, J., 2008. Measurement of the elastic properties and intrinsic strength of monolayer graphene. *science*, *321*(5887), pp.385-388.

Chapter 4

4.1 Nanofabrication of graphene spin valve with Permalloy island

NPGS is used for pattern generation and run file creation. Patterns are created using DesignCAD and Run file editor is used for alignment purposes and to record the exposure conditions. Once a design file is created using DesignCAD, pattern writing can be realized using the run file editor. Alignment can be done either automatically or manually. We prefer to use manual alignment mode where the user needs to position the alignment overlay manually to match up with the alignment marks [1]. Alignment marks are shown in Figure 33 and 34. Fabrication of a lateral graphene spin valve with Permalloy islands grown on graphene is discussed in the next paragraph which required 3 consecutive e-beam lithography steps as shown in Figure 35.

Fabrication starts with the exfoliation of graphene on a Si wafer with a 300 nm SiO_2 layer on top as shown in Figure 36. Graphene is located on the silicon substrate with an optical microscope. The next step is spin coating the substrate with MMA/PMMA at 3000rpm and bake on hot plate for 2 min at 150^{o}C and 20 min at 170^{o}C, respectively. Alignment marks are defined using e-beam lithography and developed in MIBK/IPA followed by DI water 1 min for each. Optical microscope is used for taking the images of the graphene and the alignment marks. This step is crucial for

alignment purposes and requires attention for precise alignment overlay. Any rotation or error while taking the optical image can result serious misalignment problems for the next lithography steps. NPGS design of the graphene spin valve is shown in Figure 37 and Figure 38. After taking the images, first step is the definition of Au electrodes as shown in Figure 39. This is followed by metal deposition and lift-off process as shown in Figure 40. Permalloy islands are defined using E-beam lithography followed by Permalloy deposition and lift-off again as shown in Figure 41 and Figure 42. Final step is the definition of Co electrodes as shown in Figure 43 and Figure 44. Further process details can be found in Appendix A and Appendix C.

By fabricating this device, we aim to measure the contact resistance of Permalloy island grown on graphene. Measured MR signals and contact resistances for different configurations are given in Appendix D. Basically, the island size should be in the same width or even very smaller than the graphene width to realize the current induced magnetization switching. However, due to fabrication complexity, we prefer to keep the island size wider than the graphene since keeping the detector size very small brings further challenges in nanofabrication processes. On the other side, these challenges can be achieved using advanced nanofabrication techniques such as multiple angle deposition which will be discussed in the next chapter.

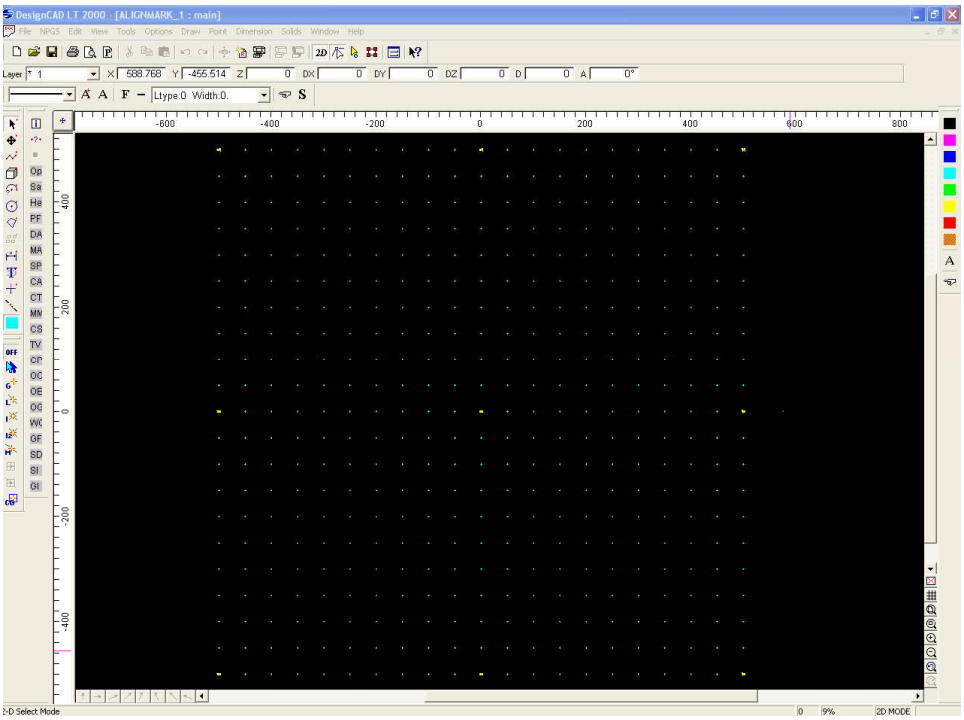

Figure 33. Alignment marks consisting of crosses and numbers.

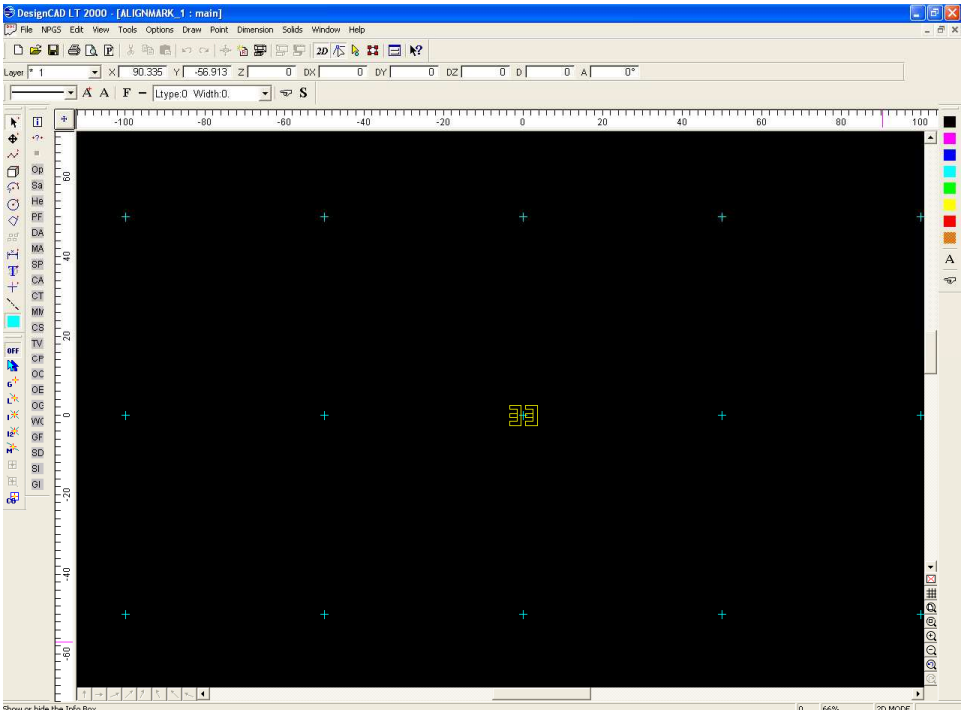

Figure 34. Alignment marks (zoomed) consisting of crosses and number.

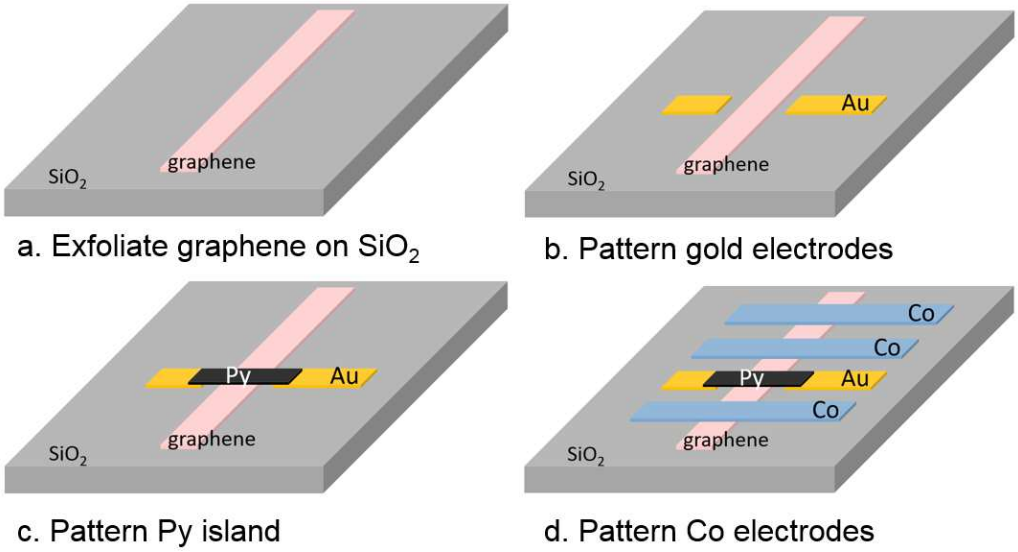

Figure 35. Nanofabrication process flow for graphene spin valve with Permalloy island.

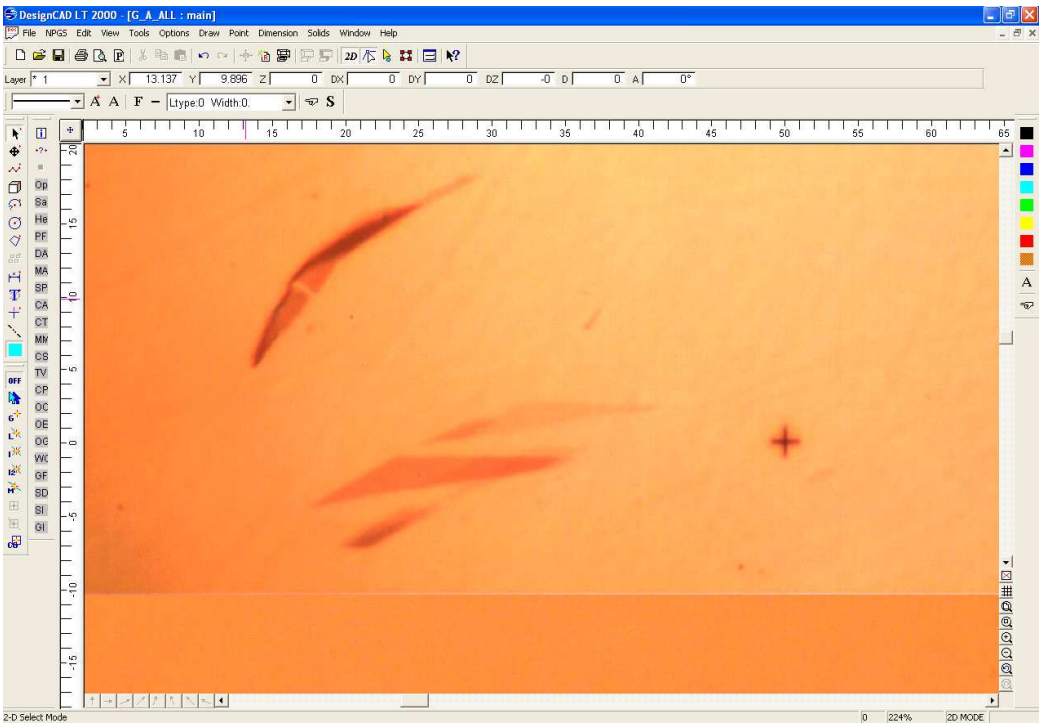

Figure 36. Exfoliated graphene on SiO_2.

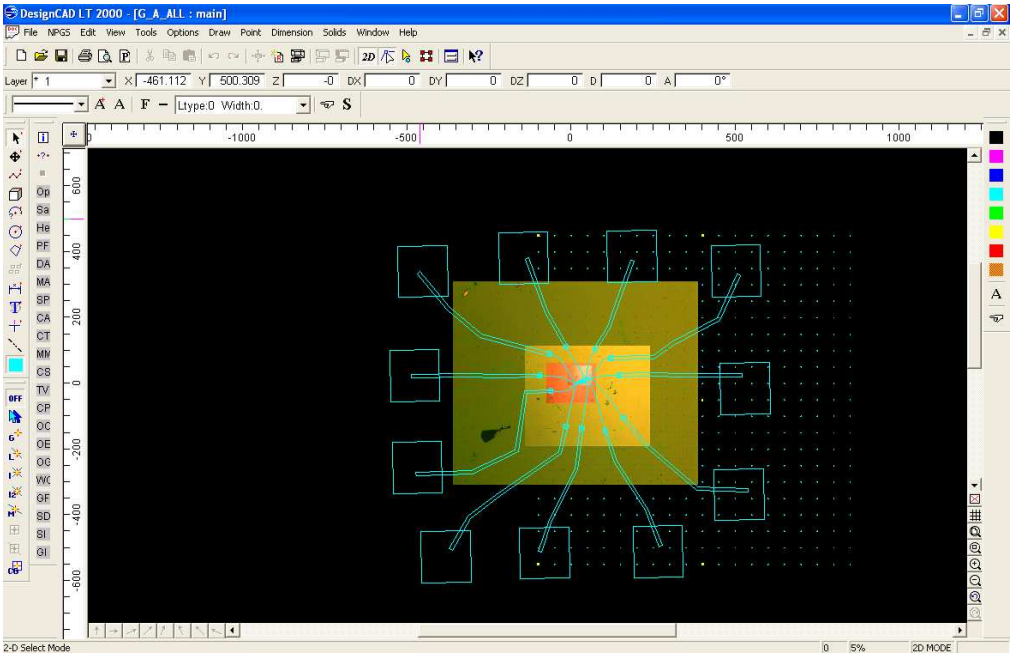

Figure 37. Spin valve design using DesignCAD software.

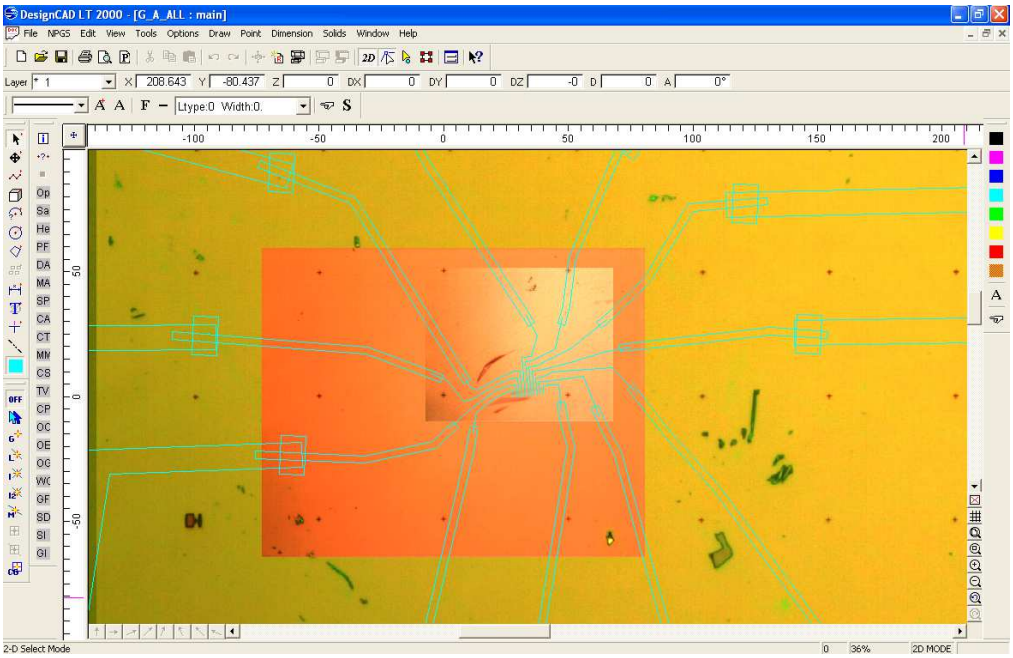

Figure 38. Spin valve design using DesignCAD software with a focus on inner electrodes.

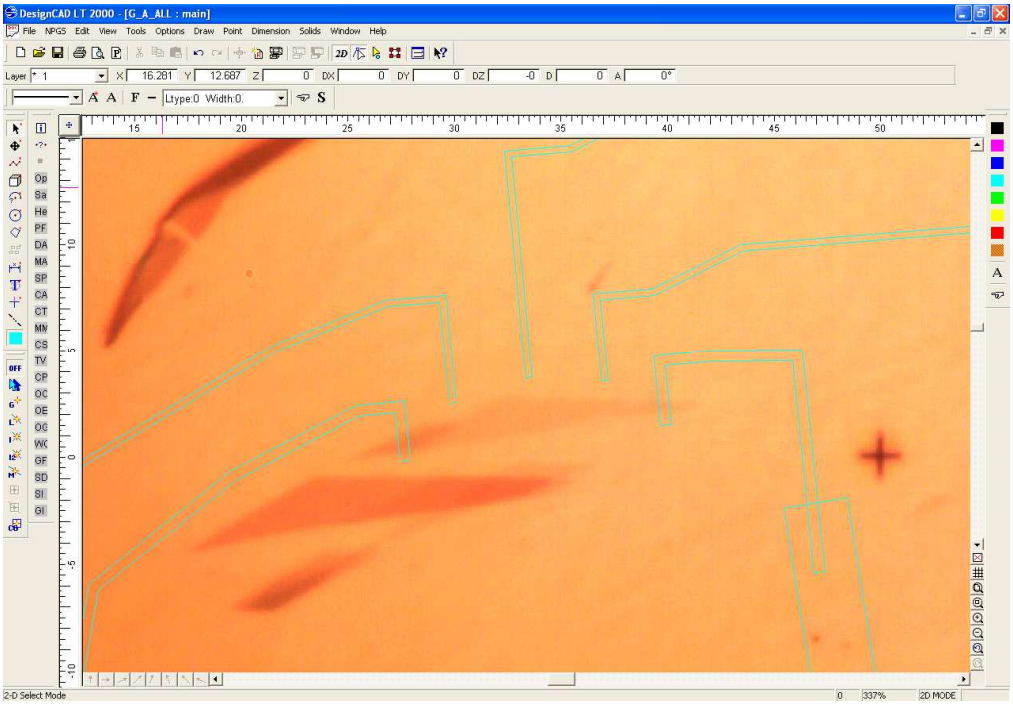

Figure 39. NPGS design of the inner Au electrodes on graphene.

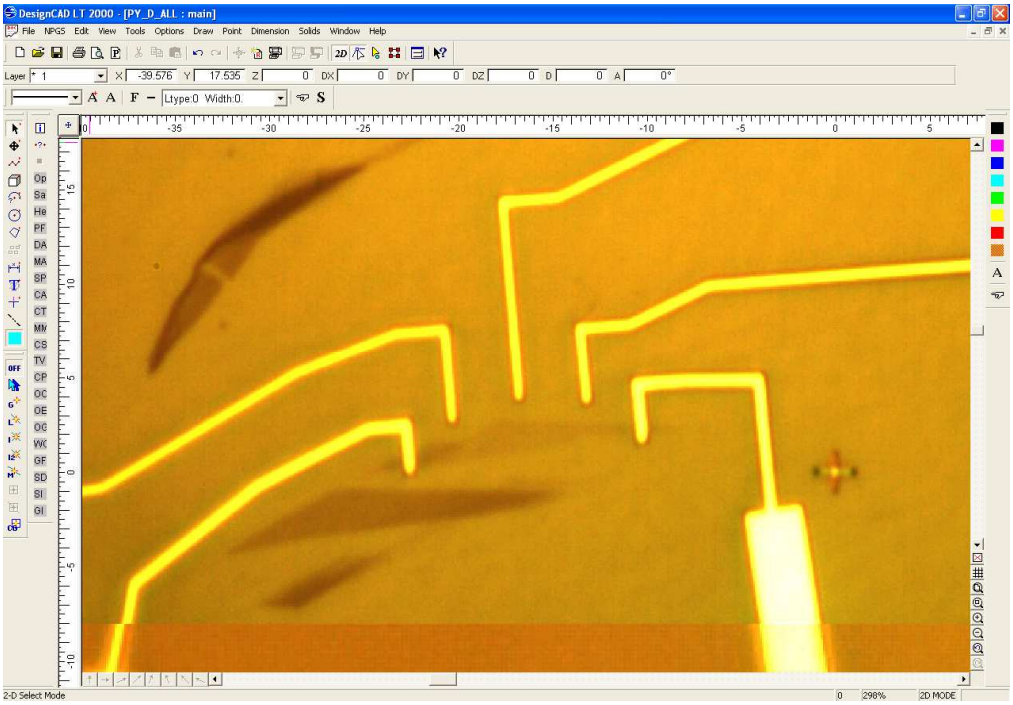

Figure 40. Inner Au electrodes on graphene after lift-off.

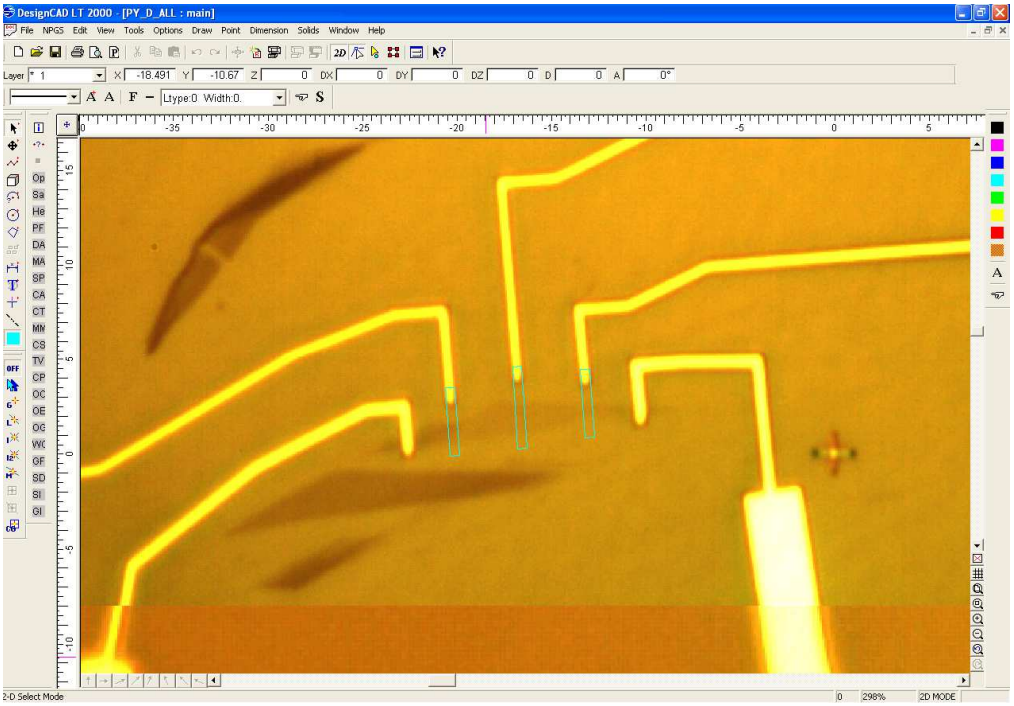

Figure 41. NPGS design of the Permalloy islands on graphene.

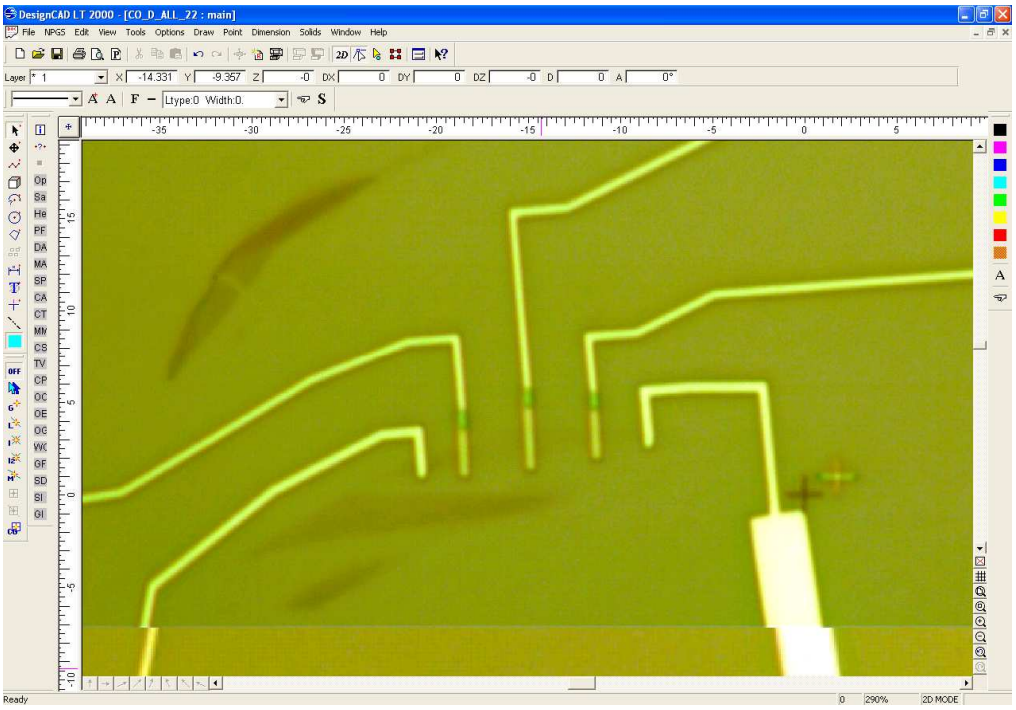

Figure 42. Permalloy islands on graphene after lift-off.

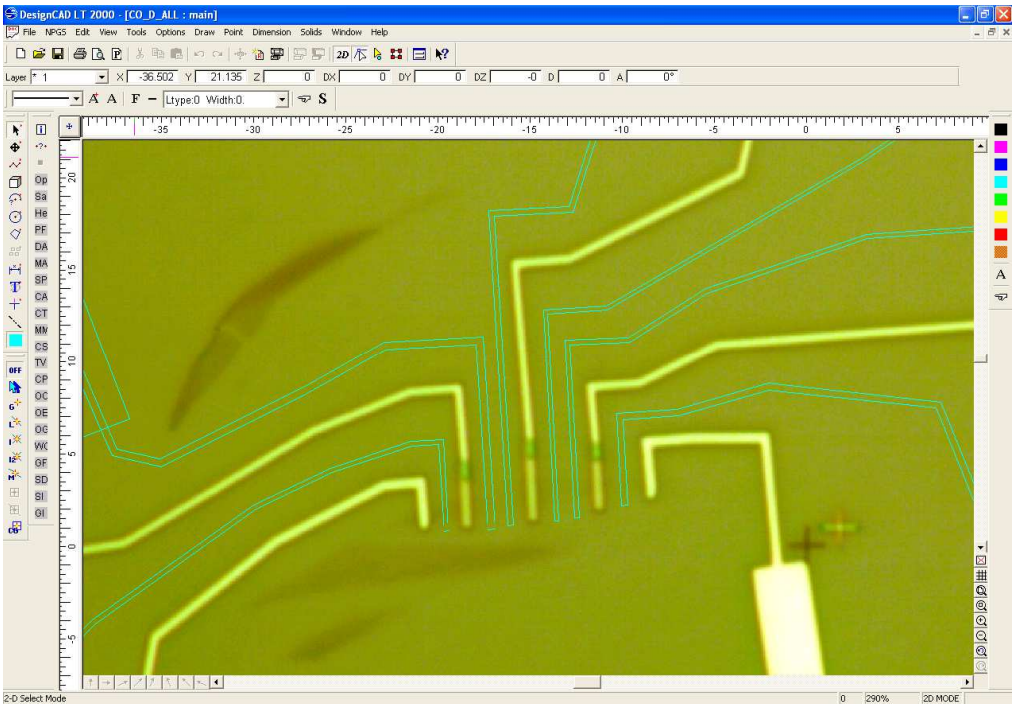

Figure 43. NPGS design of the Co electrodes on graphene.

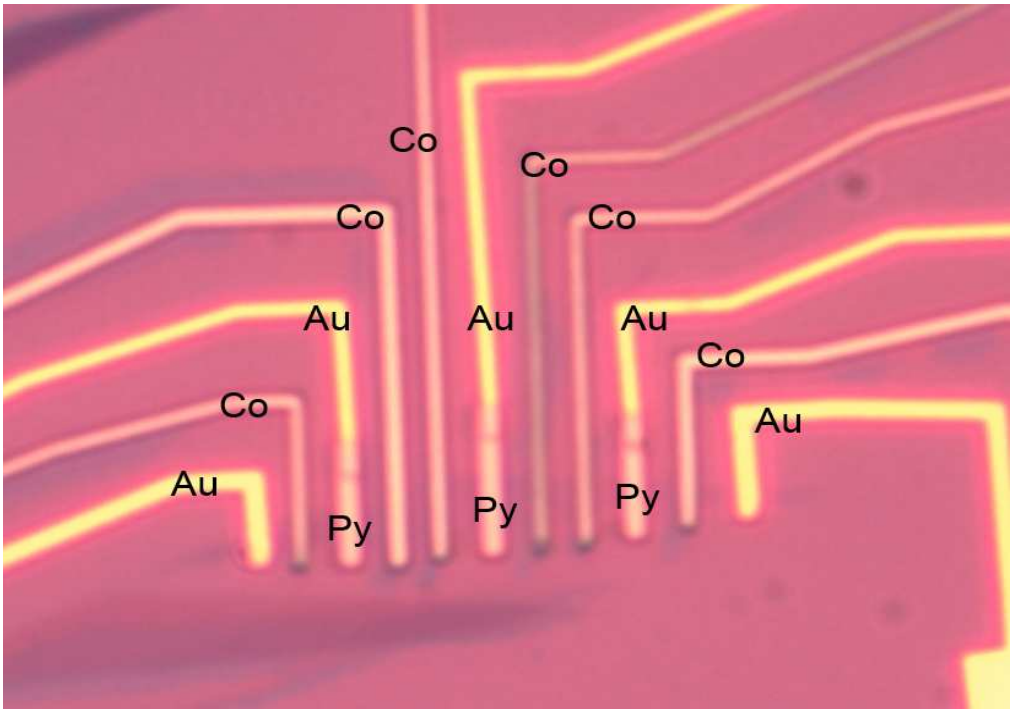

Figure 44. Optical image of the graphene spin valve with Permalloy islands.

References

[1] J. C. Nabity Lithography Systems, User's Manual for NPGS v8 & v9, 12/2002, Copyright 1988-2002.

Chapter 5

5.1 Process development for the realization of current induced magnetization switching in a lateral graphene spin valve

Spin transfer torque in graphene was first demonstrated in a lateral graphene spin valve by pure spin diffusion currents from the input ferromagnetic contact with an assisted external magnetic field [1][2]. A soft magnetic material Permalloy is used for the ferromagnetic contact for both injector and detector electrodes and Au is used for the reference electrode. The detector electrode to be switched is scaled down to 5 nm which is critical for easy switching. 4.5 mA DC current pulse for 5 μs with an assisted in plane external magnetic field of 4 mT switch the magnetization of the detector electrode. However, field assisted switching does not provide practical value. Thus, we aim to eliminate the field assisted switching by keeping the detector size very small and this brings further challenges in nanofabrication processes. Basically, the island size should be in the same width or even very smaller than the graphene width to ease the switching. Considering the nanofabrication capabilities, we aim to keep the graphene channel width as 150 nm and island width as 300 nm so that all the spins in the island can be absorbed, apply torque to the island and switch the magnetization as shown in Figure 45. Spin absorption can be achieved by only one condition that the contact

resistance of the island should be smaller than the channel resistance. Besides, advanced nanofabrication techniques such as angle evaporation is needed for the realization of the current induced magnetization.

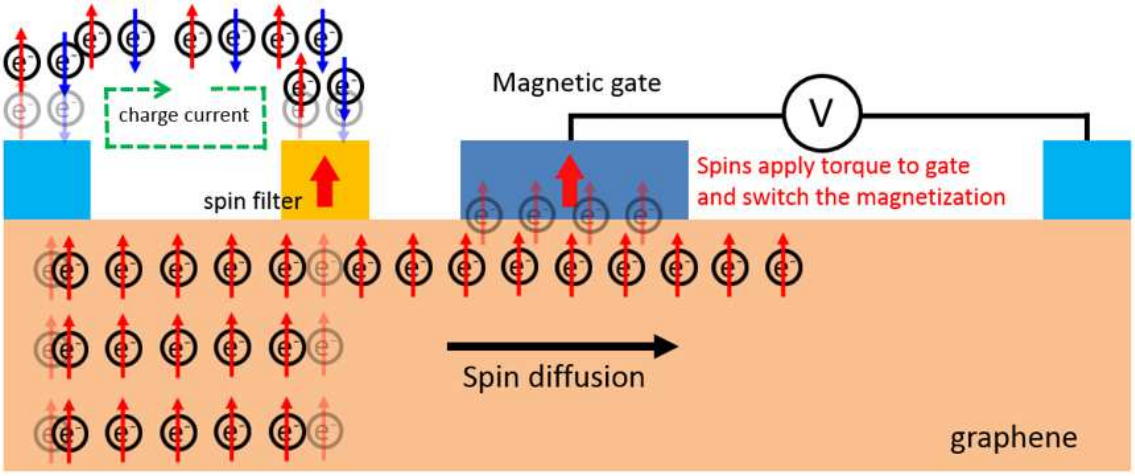

Figure 45. Schematic of the current induced magnetization switching for a lateral graphene spin valve structure.

Fabrication starts with the exfoliation of graphene on SiO_2 wafer which is followed by graphene etching step to define the borders of the graphene channel. Nanofabrication process flow is given in Figure 46. Injection electrodes are defined by e-beam lithography. Al is sputtered and oxidized in the chamber for 30 min with oxygen which results in 1 nm Al_2O_3 as a tunnel barrier. This is followed by Py deposition using MBE. Py electrodes are capped with 7 nm Al_2O_3 for preventing further oxidation afterwards. Next steps include the deposition of the Permalloy island and the contact electrode which requires two more consecutive lithography steps; one for the definition of Permalloy island and the other for the contact electrode

as shown in Figure 46-d. Instead, we use multiple angle evaporation technique [3] by which we can achieve both steps in one lithography step to eliminate the oxidation of Permalloy and also to ease the alignment steps. This is achieved by angle evaporation by taking the advantage of the resist walls. Angle evaporation steps are shown in Figures 47-Figure 52.

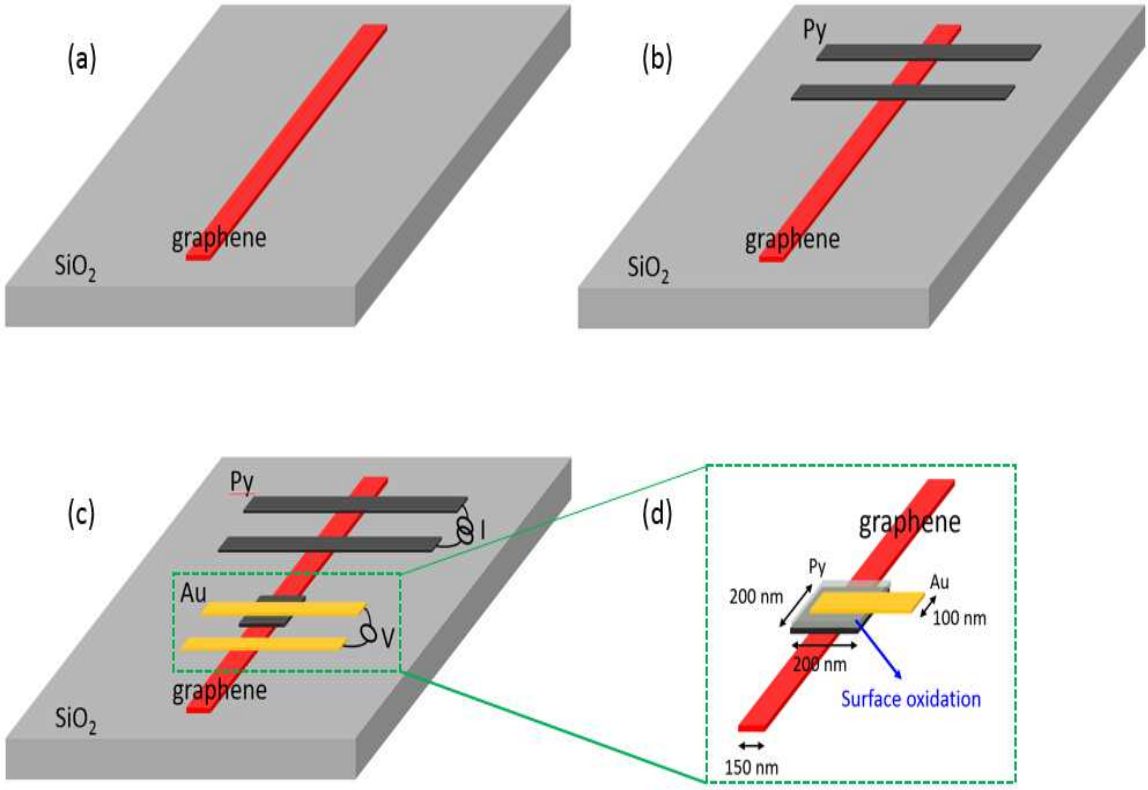

Figure 46. Nanofabrication process flow for non-local lateral spin transfer torque device on graphene. (a) Exfoliation and patterning of graphene. (b) Deposition of Permalloy injector electrode. (c-d) Permalloy and gold electrode deposition using angle evaporation.

E-beam resist is developed in such a way that two consecutive deposition steps can be realized with one lithography step as shown in Figure 47. First, Permalloy deposition is realized with an in-plane angle of 45^{o}. This

results in Permalloy deposition on a specific area while other parts are protected by the resist walls. Next step is the deposition of gold electrode with an in-plane angle of 21° so that gold is deposited on certain areas again. This is followed by regular lift-off process in acetone. Figure 53 shows the SEM image of successful fabrication of Permalloy island and crossing reference gold electrode using angle evaporation.

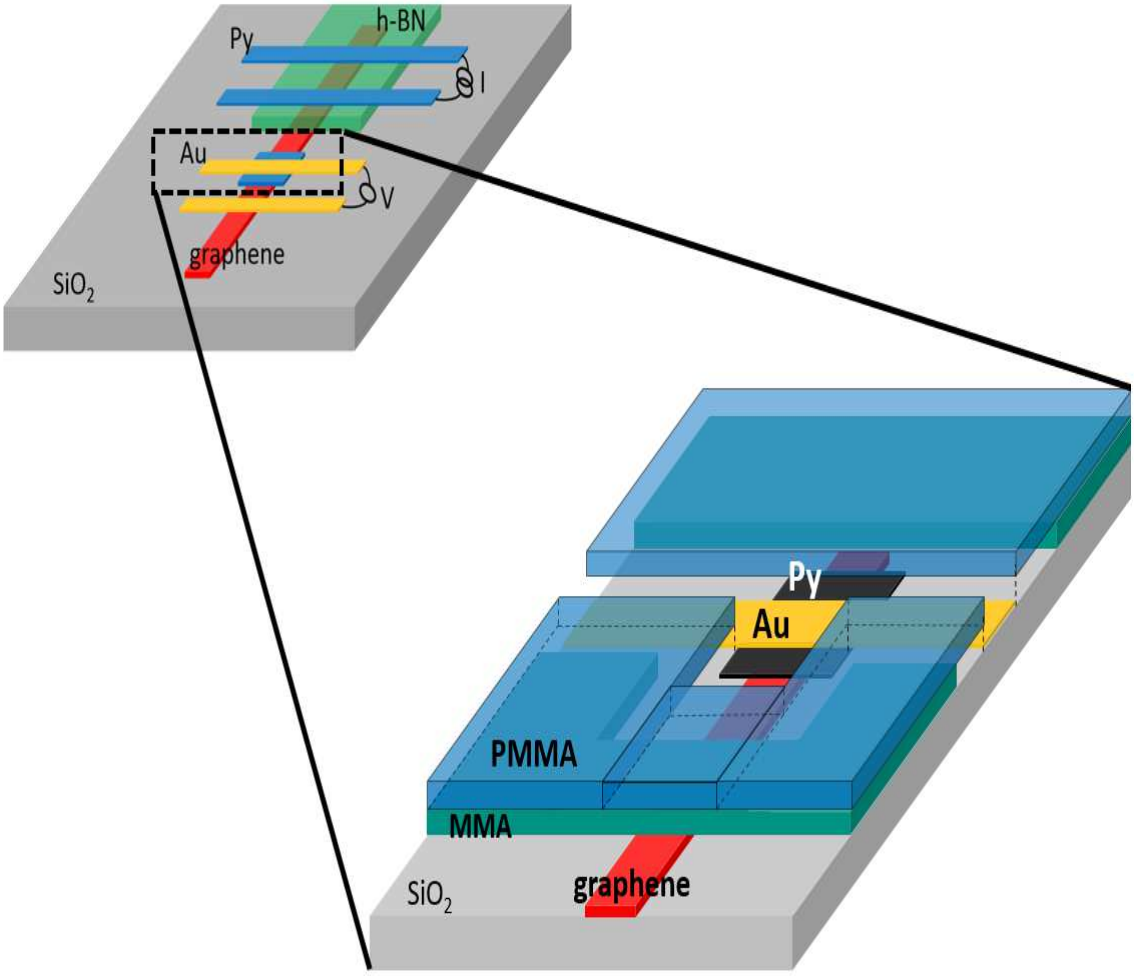

Figure 47. Schematic for angle evaporation with resist profile.

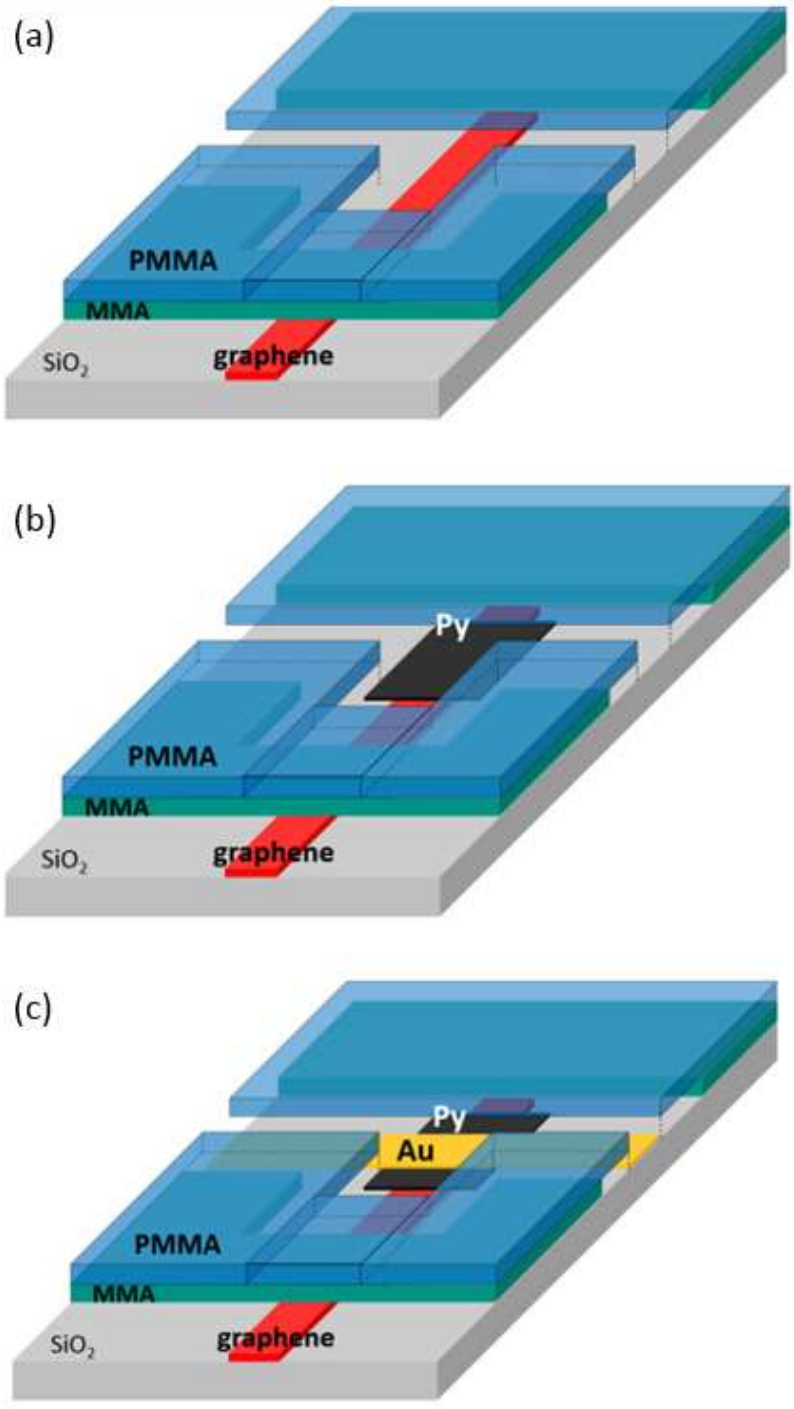

Figure 48. Nanofabrication process flow for angle evaporation of Permalloy and gold.

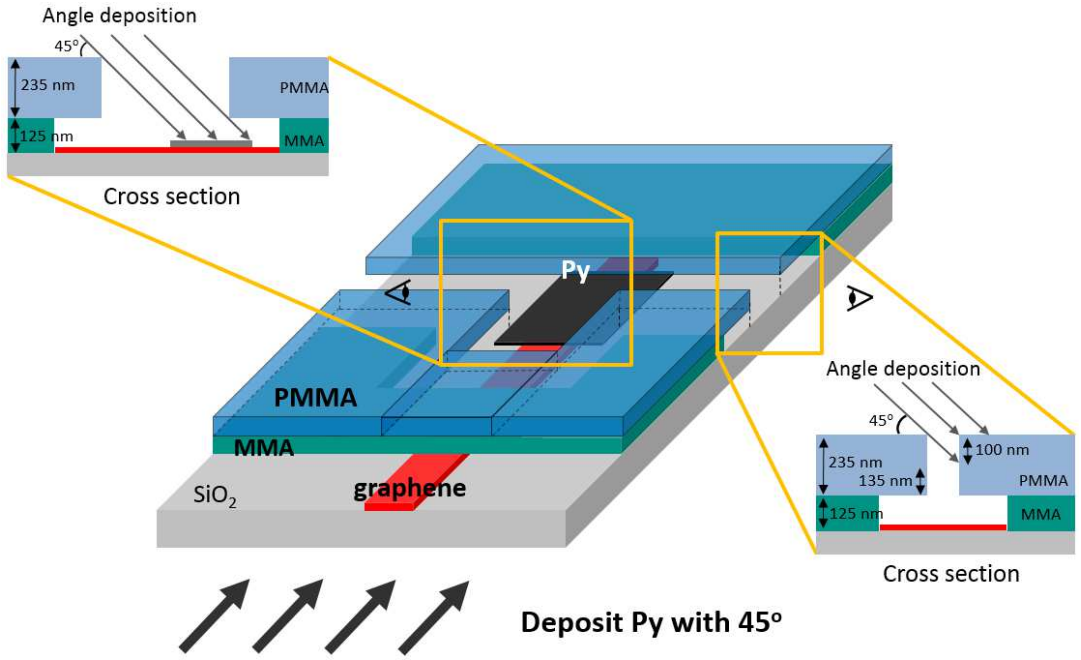

Figure 49. Schematic of angle evaporation for Permalloy with in-plane angle 45°.

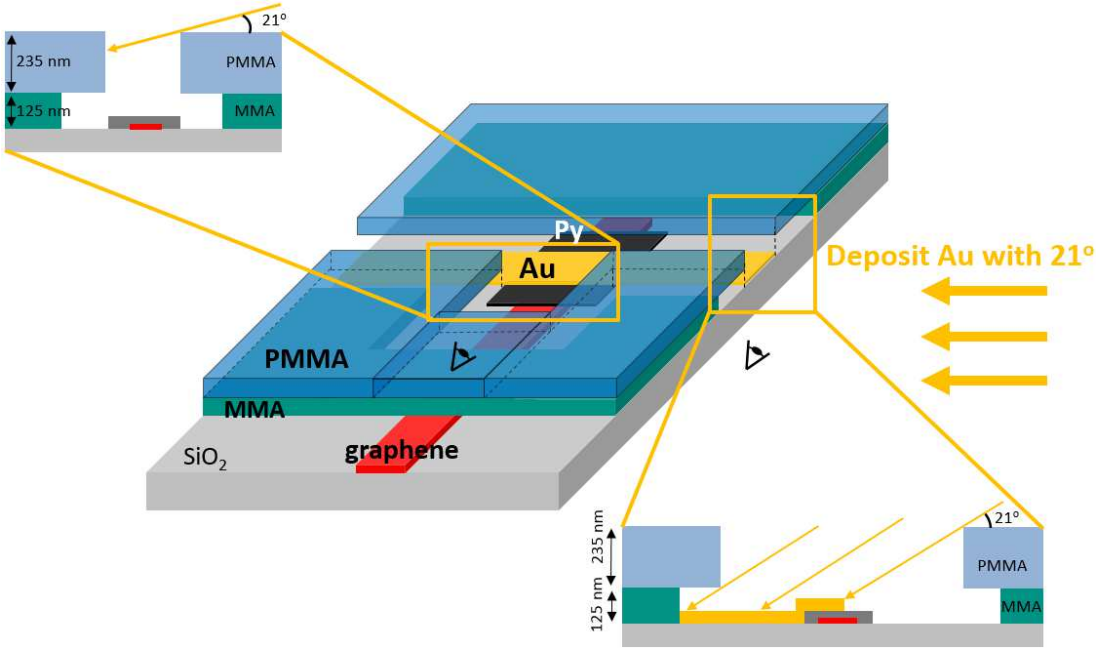

Figure 50. Schematic of angle evaporation for gold with in-plane angle 21°.

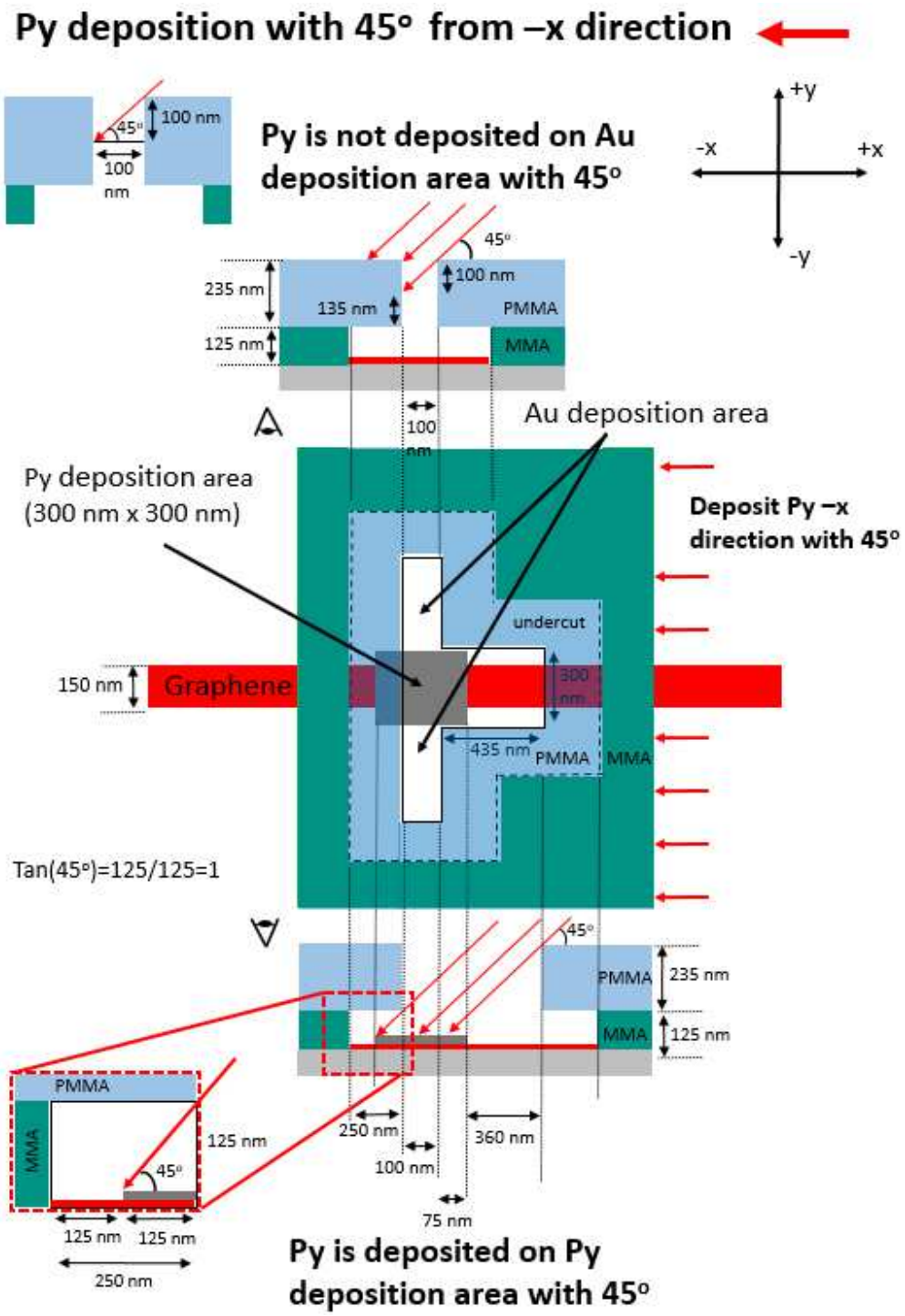

Figure 51. Process details and parameters for angle evaporation of Permalloy.

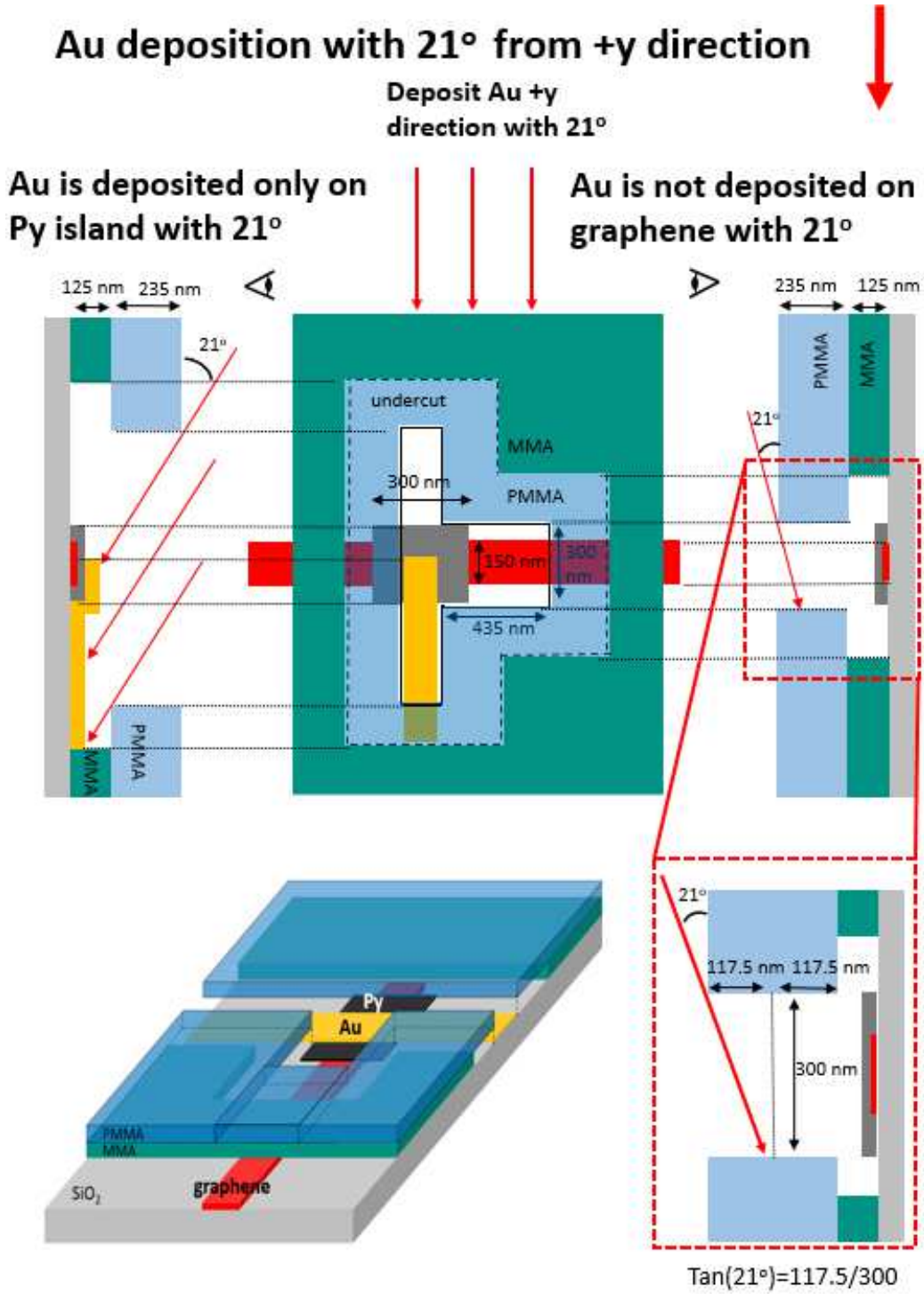

Figure 52. Process details and parameters for angle evaporation of gold electrode.

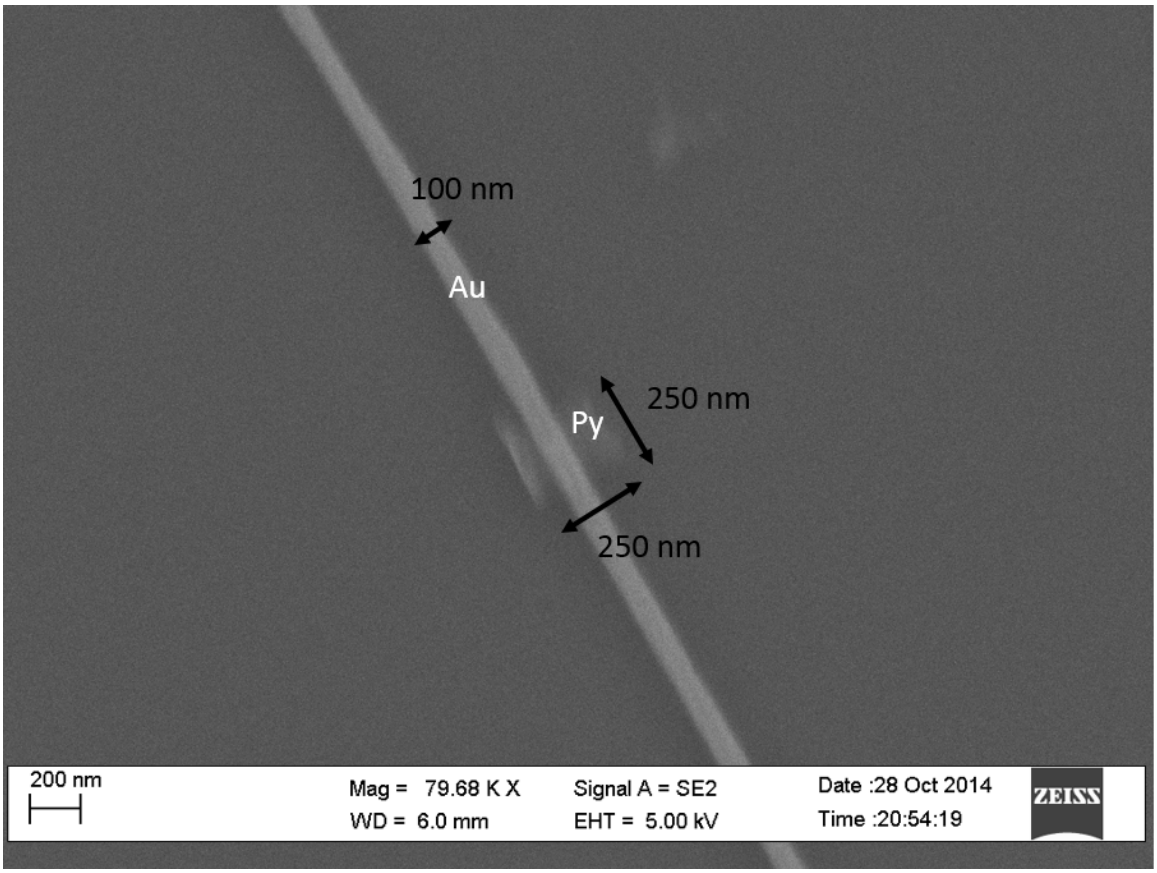

Figure 53. SEM image of Permalloy island with crossing gold electrode.

References

[1] Lin, C.C., Penumatcha, A.V., Gao, Y., Diep, V.Q., Appenzeller, J. and Chen, Z., 2013. Spin transfer torque in a graphene lateral spin valve assisted by an external magnetic field. *Nano letters*, *13*(11), pp.5177-5181.

[2] Lin, C.C., Gao, Y., Penumatcha, A.V., Diep, V.Q., Appenzeller, J. and Chen, Z., 2014. Improvement of spin transfer torque in asymmetric graphene devices. *ACS nano*, *8*(4), pp.3807-3812.

[3] Łączkowski, P., Vila, L., Ferry, S., Marty, A., George, J.M., Jaffrès, H., Fert, A., Kimura, T., Yang, T., Otani, Y. and Attané, J.P., 2011. Spin signal in metallic lateral spin valves made by a multiple angle evaporation technique.*Applied physics express*, *4*(6), p.063007.

Future work

Further experiments are required for the verification of spin absorption in graphene. The hysteric behavior can be explained in terms of the change in spin resistance due to longitudinal and transverse spin absorption happening concurrently due to inhomogeneous magnetization contributions from micro domains within the Permalloy island. This might be due to the roughness of the interface between the Py island and the graphene which overcomes the shape anisotropy of the island. Spin absorption can be characterized by the decrease in the MR signal and spin resistance determines the magnitude of the spin absorption. However, further investigation is required to correlate the result to the non-local MR measurement. Magnetic force microscopy of the island is needed in order to further confirm the observed non-local signal in our devices. Thickness dependence of the Permalloy island on the MR signal is being studied for further investigation of the spin absorption in graphene. Angle dependent spin absorption should also be investigated for further verification of transverse and longitudinal spin absorption.

Appendix A

Nanofabrication process flow details

Electron beam lithography and device fabrication

1. Start with a silicon wafer with a 300 nm SiO_2 layer.
2. Cut the wafer into small pieces for E-beam lithography with diamond pen
3. Clean wafer pieces by ultrasonic cleaning in Acetone and IPA
    a. 10 min sonication in Acetone
    b. 10 min sonication in IPA
    c. 150^{o}C on hot plate for 30 min
4. Exfoliate using MoS_2 crystal on wafer using scotch tape
5. Locate the exact location of the MoS_2 flake using optical microscope
6. Pattern alignment marks
    a. Spin coat with MMA (8.5) MAA EL 6
        i. Step 1:
            1. Ramp:500 rpm
            2. Speed:3000 rpm
            3. Time: 45 sec
        ii. Step 2:
            1. Ramp:500 rpm
            2. Speed:0 rpm
            3. Time: 2 sec

iii. 150^{o}C on hot plate for 2 minutes

b. Coat with 950 PMMA A4

i. Step 1:

1. Ramp:500 rpm
2. Speed:3000 rpm
3. Time: 45 sec

ii. Step 2:

1. Ramp :500 rpm
2. Speed:0 rpm
3. Time: 2 sec

iii. 170 ^{o}C on hot plate for 20 minutes

c. Run the NPGS file to write the alignment marks

i. Small patterns:

1. Beam size: 20μm
2. Measured beam current:130pA
3. Area dose: 500μC/cm2

ii. Large patterns:

1. Beam size: 120μm
2. Measured beam current:2580pA
3. Area dose: 500μC/cm2

d. Development

i. Develop in MIBK for 70 secs.

ii. Dip in IPA for 70 secs.

iii. Rinse in DI water for 70 secs.

7. Blow with Nitrogen very gently
8. Check the development under optical microscope
9. Deposit metal in e-beam evaporation
10. Lift-off in acetone for 30-45 min
11. Rinse in IPA and water for 1 min
12. Check the pattern under microscope

Appendix B

MoS_2 top gate transistor nanofabrication recipe

Alignment Mark Patterning	Sample Preparation	Ultrasonic cleaning in Acetone and IPA for 10 min each, heat treatment on hotplate at 150°C for 30 min
	Lithography	
	MMA Spin	MMA@3000 rpm, t=45s. (ramp:500 rpm)
	Softbake	Softbake @150°C for 2 mins. on hot plate
	PMMA Spin	PMMA@3000 rpm, t=45s. (ramp:500 rpm)
	Softbake	Softbake @170°C for 20 mins. on hot plate
	E-Beam Lithography	Pattern alignment marks (small cross patterns) Beam Size: 20 μm measured beam current: 130 μA Area Dose: 500 μC/cm^2
	E-Beam Lithography	Pattern alignment marks (Larger square patterns) Beam Size: 120 μm measured beam current: 2580 μA Area Dose: 500 μC/cm^2

	Develop	MIBK 70 secs. IPA 70 secs. DI water 70 secs.
	Ti e-beam evaporation	20 nm Ti evaporation
	Au e-beam evaporation	200 nm Au evaporation (Au evaporation is required for further alignment steps)
	Lift-off	Lift-off in acetone for 1 hour

Source and Drain Contacts	Lithography	
	MMA Spin	MMA@3000 rpm, t=45s. (ramp:500 rpm)
	Softbake	Softbake @150^{o}C for 2 mins. on hot plate
	PMMA Spin	PMMA@3000 rpm, t=45s. (ramp:500 rpm)
	Softbake	Softbake @170^{o}C for 20 mins. on hot plate
	E-Beam Lithography	Alignment using prior alignment marks
	E-Beam Lithography	Pattern source and drain (small patterns) Beam Size: 20 μm measured beam current: 50 μA Area Dose: 200 μC/cm^2
	E-Beam Lithography	Alignment using prior alignment marks
	E-Beam Lithography	Pattern source and drain contacts (Large patterns) Beam Size: 120 μm measured beam current: 2580 μA Area Dose: 500 μC/cm^2
	Develop	MIBK 70 secs. IPA 70 secs. DI water 70 secs.

	Ti e-beam evaporation	10 nm Ti evaporation
	Au e-beam evaporation	80 nm Au evaporation
	Lift-off	Lift-off in acetone for 1 hours

Dielectric Deposition	Lithography	
	MMA Spin	MMA@3000 rpm, t=45s. (ramp:500 rpm)
	Softbake	Softbake @150^{o}C for 2 mins. on hot plate
	PMMA Spin	PMMA@3000 rpm, t=45s. (ramp:500 rpm)
	Softbake	Softbake @170^{o}C for 20 mins. on hot plate
	E-Beam Lithography	Alignment using prior alignment marks
	E-Beam Lithography	Pattern dielectric area (Large pattern) Beam Size: 120 μm measured beam current: 2580 μA Area Dose: 500 μC/cm^2
	Develop	MIBK 70 secs. IPA 70 secs DI water 70 secs
	HfO_2 dielectric ALD step	30 nm HfO_2 ALD (takes about 4.5 hours)
	Lift-off	Lift-off in acetone for 1 hour

Top gate Contacts	Lithography	
	MMA Spin	MMA@3000 rpm, t=45s. (ramp:500 rpm)
	Softbake	Softbake @150^{o}C for 2 mins. on hot plate
	PMMA Spin	PMMA@3000 rpm, t=45s. (ramp:500 rpm)
	Softbake	Softbake @170^{o}C for 20 mins. on hot plate
	E-Beam Lithography	Alignment using prior alignment marks
	E-Beam Lithography	Pattern top gate metal (small pattern) Beam Size: 30 µm Measured beam current: 50 µA Area Dose: 200 µC/cm^2
	E-Beam Lithography	Alignment using prior alignment marks
	E-Beam Lithography	Pattern top gate metal contact (large pattern) Beam Size: 120 µm Measured beam current: 2580 µA

		Area Dose: 500 μC/cm^2
	Develop	MIBK 70 secs. IPA 70 secs. DI water 70 secs.
	Ti e-beam evaporation	10 nm Ti evaporation
	Au e-beam evaporation	200 nm Au evaporation
	Lift-off	Lift-off in acetone for 1 hour

Appendix C

Nanofabrication process flow for lateral graphene spin valve

Alignment Mark	Sample Preparation	Ultrasonic cleaning in Acetone and IPA for 10 min each, heat treatment on hotplate at 150^{o}C for 30 min
	Lithography	
	MMA Spin	MMA@3000 rpm, t=45s. (ramp:500 rpm)
	Softbake	Softbake @150^{o}C for 2 mins. on hot plate
	PMMA Spin	PMMA@3000 rpm, t=45s. (ramp:500 rpm)
	Softbake	Softbake @170^{o}C for 20 mins. on hot plate
	E-Beam Lithography	Pattern alignment marks (small patterns) Beam Size: 20 µm Measured beam current: 130 µA Area Dose: 500 µC/cm^2
	E-Beam Lithography	Pattern alignment marks (Larger patterns) Beam Size: 120 µm Measured beam current: 2580 µA Area Dose: 500 µC/cm^2
	Optical microscope	Optical image upload into NPGS system

	E-beam lithography	Alignment by previously patterned alignment marks
	E-beam lithography	Pattern Cobalt electrodes on exfoliated graphene Beam Size: 20 μm measured beam current: 50 μA Area Dose: 200 μC/cm^2
	Develop	MIBK 70 secs. IPA 70 secs. DI water 70 secs.
	Co deposition	80 nm Co deposition using MBE
	Lift-off	Lift-off in acetone for 1 hours

Appendix D

MR signals and contact resistance measurements for different electrode configurations in a lateral graphene spin valve

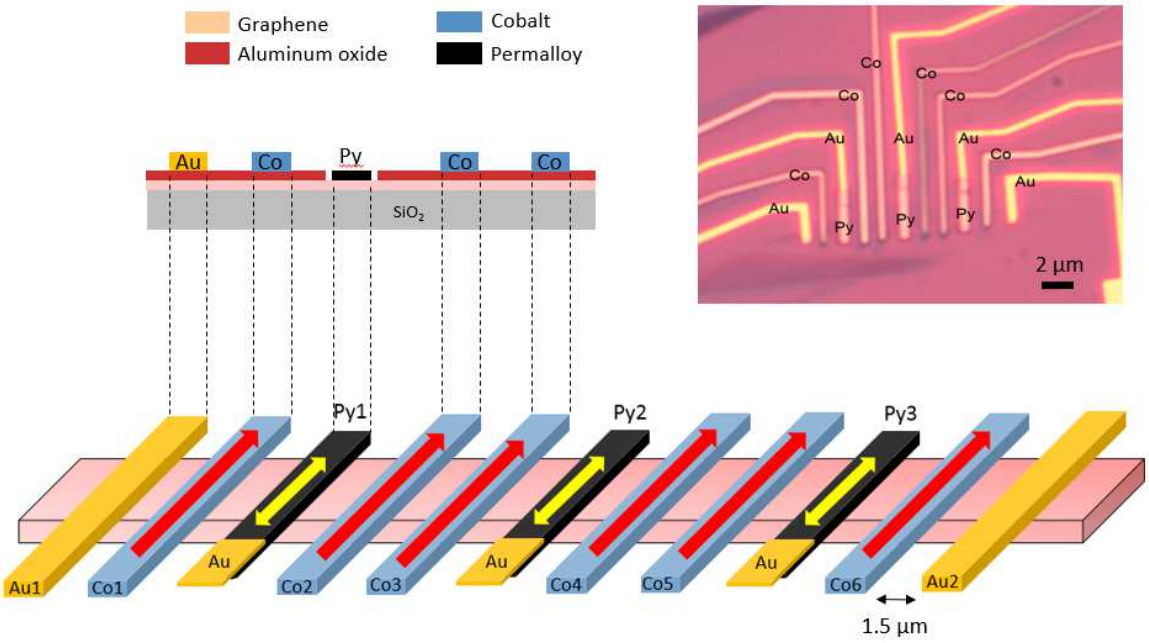

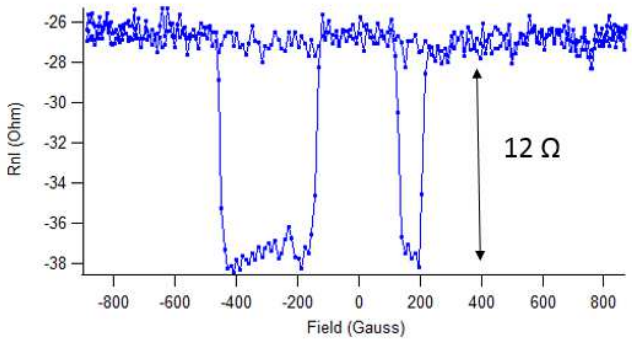

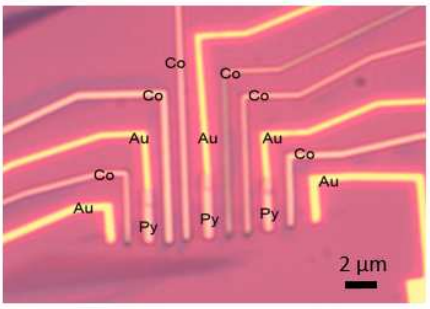

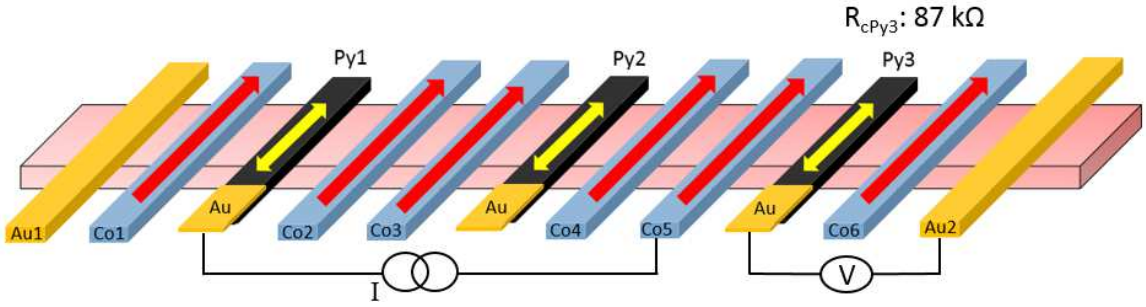

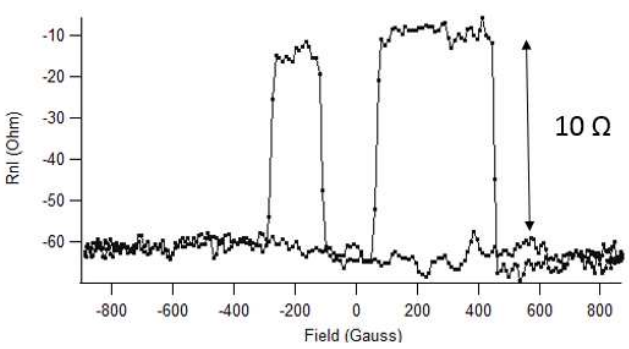

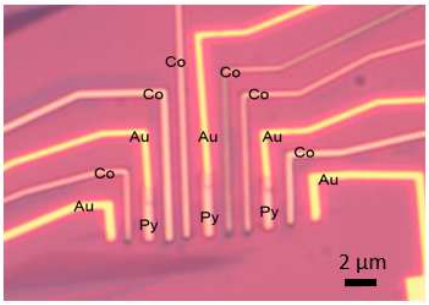

R_{cPy2}: 40 kΩ

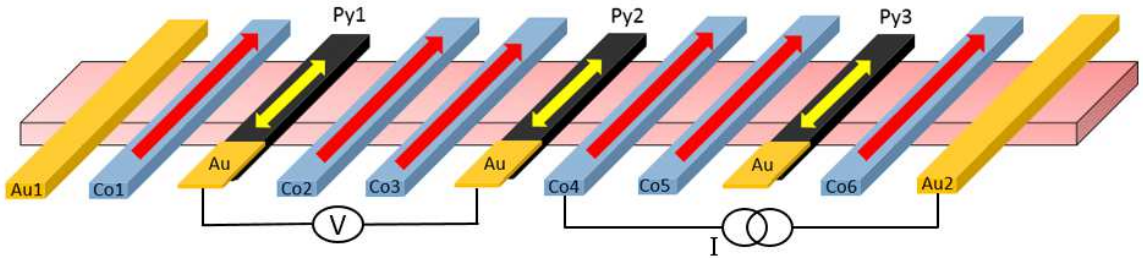

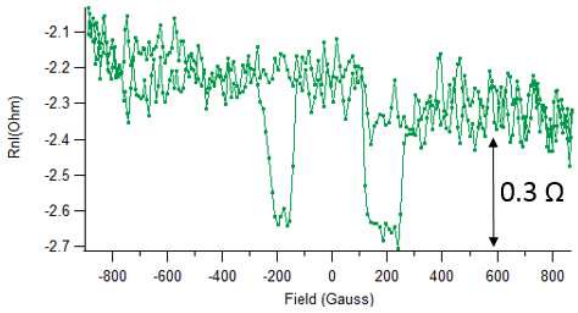

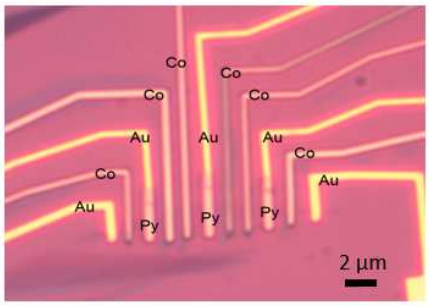

R_{cPy1}: 14 kΩ

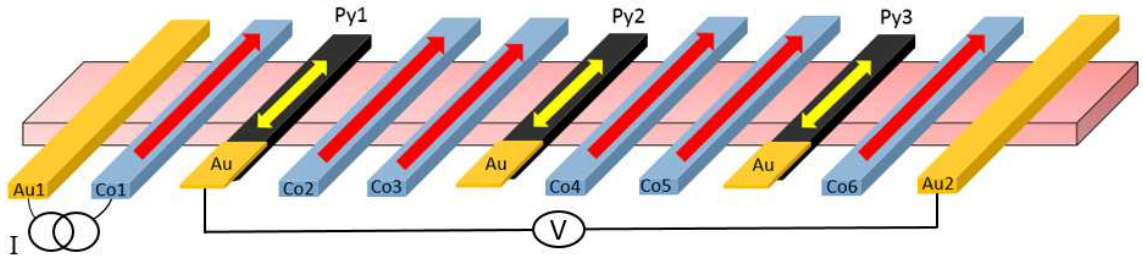

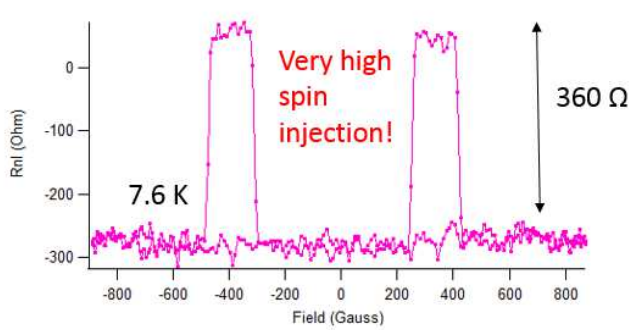
Very high
spin
injection!
360 Ω
7.6 K
Rnl (Ohm)
Field (Gauss)

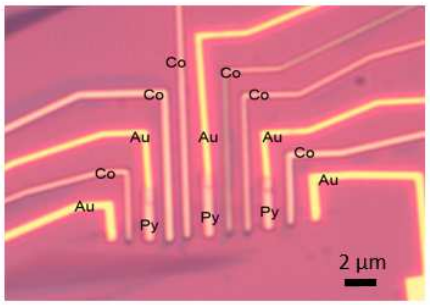
Co
Au
Py
2 µm

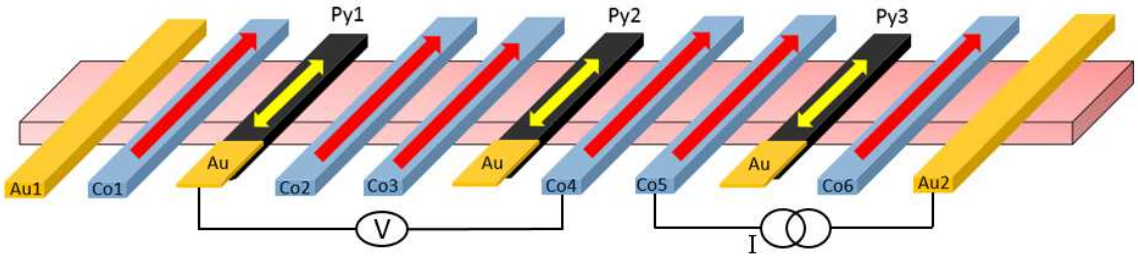
Py1
Py2
Py3
Au1
Co1
Au
Co2
Co3
Co4
Co5
Co6
Au2
V
I

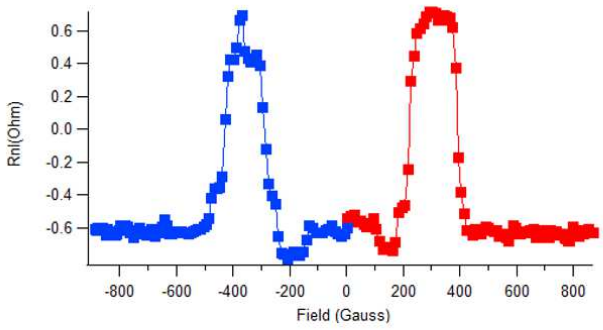
Rnl(Ohm)
Field (Gauss)

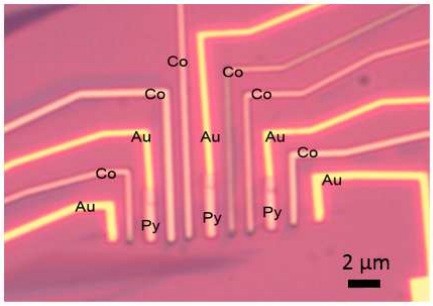
Co
Au
Py
2 µm

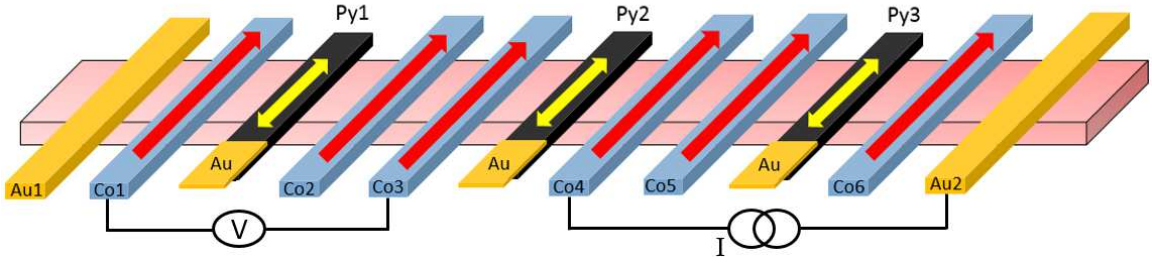
Py1
Py2
Py3
Au1
Co1
Au
Co2
Co3
Co4
Co5
Co6
Au2
V
I